REPORT DOCUMENTATION PAGE

Form Approved
OMB No. 0704-0188

1. REPORT DATE *(DD-MM-YYYY)*	2. REPORT TYPE	3. DATES COVERED *(From - To)*
02-05-2006	Final Technical Report	01-09-2002/31-08-2005

4. TITLE AND SUBTITLE
A Stress Gradient Failure Theory for Textile Structural Composites

5a. CONTRACT NUMBER
00034750

5b. GRANT NUMBER
DAAD19-02-1-0330

5c. PROGRAM ELEMENT NUMBER

6. AUTHOR(S)
Bhavani V. Sankar and Ryan L. Karkkainen

5d. PROJECT NUMBER
PR 00025560

5e. TASK NUMBER

5f. WORK UNIT NUMBER

7. PERFORMING ORGANIZATION NAME(S) AND ADDRESS(ES)
University of Florida
Mechanical and Aerospace Engineering
223 Grinter Hall
Gainesville FL 32611-1582

8. PERFORMING ORGANIZATION REPORT NUMBER

9. SPONSORING / MONITORING AGENCY NAME(S) AND ADDRESS(ES)
US Army Research Office
P.O. Box 12211
Research Triangle Park, NC
27709-2211

10. SPONSOR/MONITOR'S ACRONYM(S)

11. SPONSOR/MONITOR'S REPORT NUMBER(S)
42688.4-EG

12. DISTRIBUTION / AVAILABILITY STATEMENT
Approved for Public Release; distribution is unlimited

13. SUPPLEMENTARY NOTES

14. ABSTRACT

Micromechanical methods for stiffness and strength prediction of textile composites are presented, the results of which have led to an effective failure theory for prediction of strength. Methods to account for analysis of multi-layer textile composites are also developed. For textile composites, effects of stress gradients are important, as the size of the representative volume element (RVE) will typically be several orders of magnitude larger than that of a unidirectional RVE. The stress state is defined in terms of the well-known laminate theory force and moment resultants [*N*] and [*M*]. Structural stiffness coefficients analogous to the [*A*], [*B*], [*D*] matrices are defined, and these are computed directly using the Direct Micromechanics Method (DMM). Based upon these results, a robust 27-term quadratic failure criterion has been developed to predict failure under general loading conditions. For multi-layer analysis, the methods are adapted via three techniques: direct simulation of a multi-layer composite, an adjustment of the data output from single-layer FEM simulation, and an adjustment of the quadratic failure theory. The adjusted single-layer data analysis and the adjusted quadratic failure criterion show 5.2% and 5.5% error over a variety of test cases.

15. SUBJECT TERMS
textile composites, failure criteria, stress gradient effects

16. SECURITY CLASSIFICATION OF:			17. LIMITATION OF ABSTRACT	18. NUMBER OF PAGES	19a. NAME OF RESPONSIBLE PERSON
a. REPORT	b. ABSTRACT	c. THIS PAGE			Bhavani V. Sankar, Ph.D.
Unclassified	Unclassified	Unclassified	UL	99	19b. TELEPHONE NUMBER *(include area code)* (352)392-6749

A Stress Gradient Failure Theory for Textile Structural Composites

Final Technical Report submitted to ARO

By

RYAN KARKKAINEN and BHAVANI SANKAR
University of Florida
Department of Mechanical & Aerospace Engineering
PO Box 116250, Gainesville, FL 32611, USA

May 2006

TABLE OF CONTENTS

page

LIST OF TABLES

LIST OF FIGURES

Abstract

A Stress Gradient Failure Theory for Textile Structural Composites

Ryan Karkkainen and Bhavani Sankar

University of Florida, Gainesville, Florida

May 2006

Micromechanical methods for stiffness and strength prediction are presented, the results of which have led to an effective failure theory for prediction of strength. Methods to account for analysis of multi-layer textile composites are also developed. This allows simulation of a single representative volume element (RVE) to be applicable to a layup of an arbitrary number of layers, eliminating the need for further material characterization. Thus a practical tool for failure analysis and design of a plain weave textile composite has been developed. These methods are then readily adaptable to any textile microarchitecture of interest.

A micromechanical analysis of the RVE of a plain-weave textile composite has been performed using the finite element method. Stress gradient effects are investigated, and it is assumed that the stress state is not uniform across the RVE. This is unlike most models, which start with the premise that an RVE is subjected to a uniform stress or strain. For textile geometries, non-uniform stress considerations are important, as the size of a textile RVE will typically be several orders of magnitude larger than that of a unidirectional RVE. The stress state is defined in terms of the well-known laminate theory force and moment resultants [N] and [M]. Structural stiffness coefficients

analogous to the [A], [B], [D] matrices are defined, and these are computed directly using the Direct Micromechanics Method (DMM), rather than making estimations based upon homogenized properties.

Based upon these results, a robust 27-term quadratic failure criterion has been developed to predict failure under general loading conditions. For multi-layer analysis, the methods are adapted via three techniques: direct simulation of a multi-layer composite, an adjustment of the data output from single-layer FEM simulation, and an adjustment of the quadratic failure theory (without the requirement of determining a new set of failure coefficients). The adjusted single-layer data analysis and the adjusted quadratic failure criterion show 5.2% and 5.5% error over a variety of test cases.

The entire body of work is then applied to several practical examples of strength prediction to illustrate their implementation. In many cases, comparisons to conventional methods show marked improvements.

CHAPTER 1
INTRODUCTION

Though composites in general are not a new material, continuing advancements in constituent materials, manufacturing techniques, and microstructures require that considerable amounts of research be devoted to the study of composite mechanics. The associated knowledge base is much smaller when compared to more conventional materials, such as metals or ceramics. Composites have yet to be absorbed into widespread use across multiple industries, limiting their economy and familiarity. Much remains to be developed in the way of design methodologies and effective employment in optimized structural applications.

By far the two most commonly employed and studied composite materials are randomly oriented chopped-fiber composites, as well as laminated polymer composites with embedded unidirectional carbon, glass, or Kevlar fibers. Such composites have received a great amount of treatment in the literature, and much exists in the way of stress analysis techniques, and effective prediction of stiffness, fatigue life, strength, and other such mechanical analyses.

Textile composites are a subgroup of composite materials that are formed by the weaving or braiding of bundles of fibers (called tows or yarns), which are resin-impregnated and cured into a finished component. Though heavily adapted, in some sense they draw upon traditional textile weaving processes and fabrication machines such as mandrels and looms, akin to those of the textile clothing industries. Much of the terminology of structural textile composites draws upon this classical sense as well.

The value of textile composites stems from many advantages, such as speed and ease of manufacture of even complex components, consequent economy compared to other composite materials, and out-of-plane reinforcement that is not seen in traditional laminated composites. Further, textile composites do not lose the classically valued advantage that composite materials possess over their metal or traditional counterparts, in that textile composites have an inherent capacity for the material itself to be adapted to the mechanical needs of the design. This is to say that the strength and stiffness of the material can be oriented in needed directions, and no material weight is wasted in providing reinforcement in unnecessary directions. For a conventional laminated composite, this is accomplished by oriented stacking of layers of unidirectional resin-impregnated fibers, such that fibers are aligned with any preferred loading axes. A textile composite may also be so adapted by several methods, such as unbalanced weaves. The woven fiber tows in a preferred direction may be larger (containing more constituent fibers per tow) than in other directions. Also, an extremely diverse set of woven or braided patterns may be employed, from a simple 2D plain weave to an eight-harness satin weave or a 3D orthogonal weave pattern, any of which may exhibit a useful bias in orientation of material properties. Figure 1-1 through Figure 1-3 [1] illustrate some of the more common of these patterns.

The economy of textile composites arises mainly from the fact that manufacturing processes can be highly automated and rapidly accomplished on loom and mandrel type machinery. This can lead to easier and quicker manufacture of a finished product, though curing times may still represent a weak link in the potential speed of manufacture.

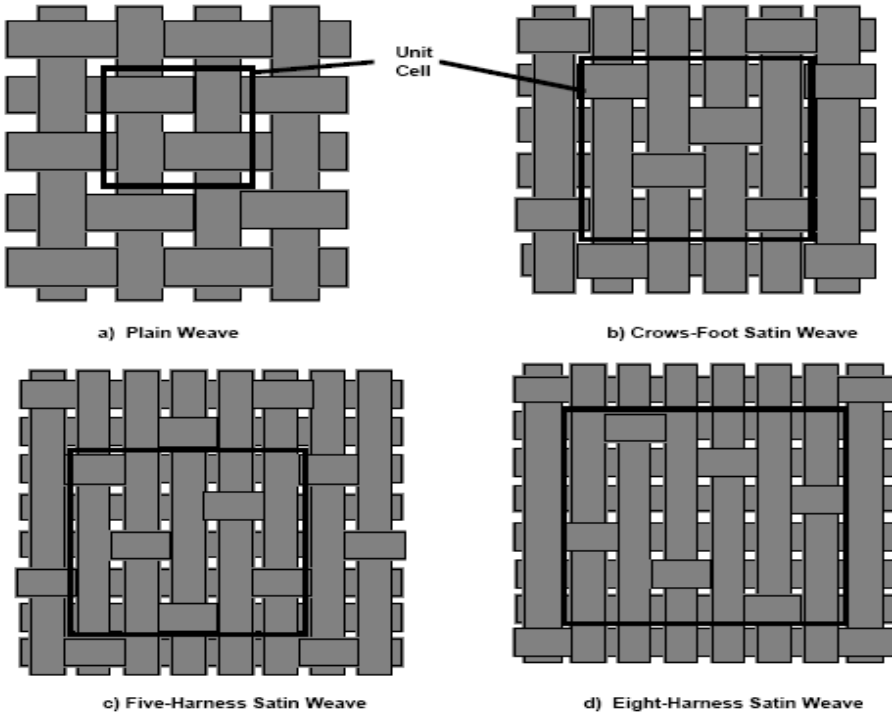

Figure 1-1. A Schematic Illustration of Several Common Weave Patterns Employed with Textile Composites. A Box Indicating the Unit Cell Borders the Smallest Repeatable Geometry Element for Each Pattern.

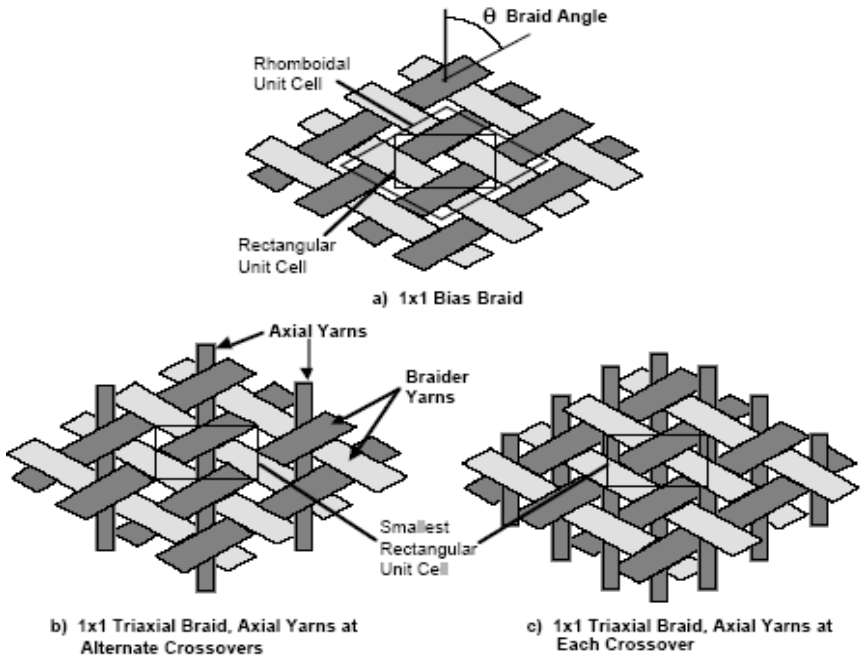

Figure 1-2. A Schematic Illustration of Several Common Braid Patterns Employed with Textile Composites. A Box Indicating the Unit Cell Borders the Smallest Repeatable Geometry Element for Each Pattern.

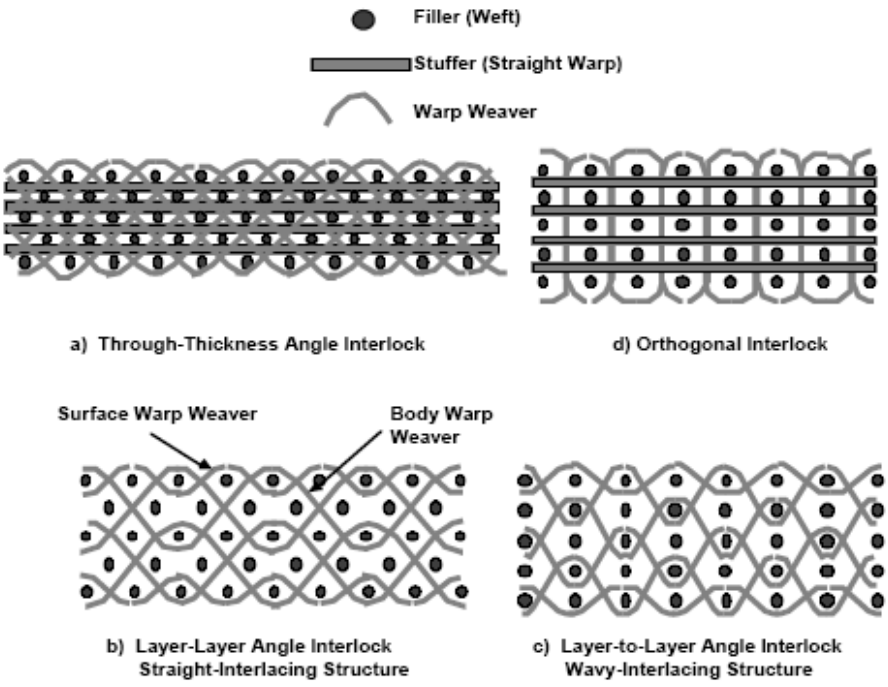

Figure 1-3. A Schematic Illustration of Several Common 3D Weave Patterns Employed with Textile Composites.

The out-of-plane reinforcement provided by textile composites comes by virtue of the fact that the constituent weave patterns lead inherently to undulation and interlacing of the woven fiber tows, which become oriented out of plane. A 2D weave will typically exhibit tow undulation varying from 0 to 15 degrees out of plane. A 3D weave such as an orthogonal interlock may actually have fiber tows directly aligned in the out of plane direction.

Naturally, there are also several tradeoffs and disadvantages associated with laminated and textile composites. The most significant added disadvantage that textile composites possess may be the increased complexity of mechanical analysis. This is directly owing to the undulation inherent to the weave or braid patterns, the complexity of microstructure, as well as the multiscale nature of the textile microstructure. The fiber tows woven together and embedded in a bulk polymer matrix are the most representative

microstructure, but the tows themselves have an inherent microstructure of aligned fibers and intra-tow polymer matrix.

Given this increased complexity of analysis, there are several outstanding issues with regards to textile composites. One of the most important issues, and the issue which is to be addressed in the current body of research, is a robust model for prediction of strength.

Current failure theories are generally developed for unidirectional composites and do not capture the unique characteristics of textile composites. Though these theories may to some extent be applied in an adapted form to the analysis of textile composites, many inherent simplifying assumptions will no longer apply, and in general such techniques will not be suitable to the increased complexity intrinsic to textile geometry. Even at the micro scale, textile composites maintain a relatively complicated microstructure. Even under simple loading conditions, a textile microstress state will be shown to be quite complex, and elastic constants are non-uniform due to the waviness of a woven fiber tow. Laminate analysis, property homogenization, and other common approaches will no longer apply. Thus, current designs of textile structures will not be optimized for maximum damage resistance and light-weight.

Conventional micromechanical models for textile composites assume that the state of stress is uniform over a distance comparable to the dimensions of the representative volume element (RVE). However, due to complexity of the weave geometry, the size of the RVE in textile composites can be large compared to structural dimensions. In such cases, severe non-uniformities in the stress state will exist, and conventional models may fail. Such stress gradients also exist when the load is applied over a very small region, as

in static contact or foreign object impact loading, and when there are stress concentration effects such as open holes in a structure.

Although micromechanical models have been successfully employed in predicting thermo-elastic constants of fiber-reinforced composite materials, their use for strength prediction in multiaxial loading conditions is not practical, as computational analysis must be performed in each loading case. Thus phenomenological failure criteria are still the predominant choice for design in industry. There are three major types of engineering failure criteria for unidirectional composite materials: maximum stress criterion, maximum strain criterion, and quadratic interaction criterion, such as the Tsai-Hill and Tsai-Wu failure theories [2].

Most of the micromechanical modeling work done thus far has focused on predicting thermo-mechanical properties [3-6]. To facilitate the use of textile composites in lightweight structures, it is required to have a lucid understanding of failure mechanisms, and design engineers must have an accurate and practical model for prediction of failure stress. Most of the current analytical and numerical methodologies developed to characterize textile composites [7-14] assume that the textile is a homogeneous material at the macroscopic scale.

Finite element analysis of initial failure of a plain weave composite [10] has shown that failure due to inter-tow normal stresses are the predominant mode of failure, and there is generally little or no damage volume of the bulk matrix between tows. This work is extended to a thorough investigation of progressive failure analysis under axial extension using several different property knockdown schemes. This has shown stiffness losses on the order of 40% after initial failure. More recently this work has been

extended to include the capability for more detailed stress fields in the RVE under investigation [15], and techniques have been developed to minimize required computation times by employing boundary conditions based on thorough exploitation of symmetry and periodicity of RVE geometry [16].

The Binary Model [17, 18] allows for quick and efficient analysis of any textile weave of interest. It has been shown to provide for accurate prediction of stiffness properties. Further, it is robust and readily adaptable to provide insight into effects of alteration of parameters such as tow waviness, tow misalignment, varying weave architectures, etc. This technique does not yield a detailed map of RVE stress fields or allow for cross-sectional variation of tow geometry, as the fiber tow is simulated as an embedded 1-D line element with representative material properties. Thus some micro-level detail is lost to provide for computational efficiency and macro-level representation.

The Mosaic Model and its adaptations [7, 19, 20] represent a textile composite RVE as a collection of homogenized blocks, each with unidirectional composite or matrix properties. These blocks are then assembled to represent the weave geometry under consideration. In this way, classical laminate plate theory can be used to determine the global stiffness matrix of the RVE. For macroscopically homogeneous load cases, good agreement has been shown with experimental data, including three-dimensional weave geometries.

Effective prediction of compressive strength of braided textile composites using a detailed FEM micromechanical model has been performed [21], which shows good comparison to experimental results in a parallel study [22]. A detailed 3D solid model was formed to exactly model a 2D triaxially braided composite RVE. Biaxial loading is

considered in both the experimental and computational analyses. Buckling analysis has been performed, and the effects of tow waviness and microarchitecture on the compressive strength are shown.

For uniaxially loaded textile composites, consistent but optimistic strength estimates have been made by comparing the strength of fiber tows with the predicted stresses in the fiber yarns that are aligned with the loading axis [23-25]. The off-axis tows are given little consideration, without much effect on the outcome, as they play little part in such uniaxial loading cases. Multi-axial loading presents an obvious escalation in modeling complexity. The failure envelope for combined transverse tension and in-plane shear has been presented as an ellipse [26], according to quadratic strength rules developed for unidirectional composites. Further, proposals for multiaxial loadings submit that axial strain in the textile geometry should be compared to a critical value of tow strain, analogous to a first-ply failure criterion for unidirectional composites [27].

A previous study [28] extended a method, known as the Direct Micromechanics Method [29] (DMM), to develop failure envelopes for a plain-weave textile composite under plane stress in terms of applied macroscopic stresses. In this study, it was assumed that the state of stress is uniform across the RVE. The micro scale stresses within the RVE were computed using finite element methods. The relation between the average macrostress and macrostrains provides the constitutive relations for the idealized homogeneous material. The microstresses are used to predict the failure of the yarn or matrix, which in turn translates to failure of the textile composite.

In the current research, micromechanical finite element analysis is performed to determine the constitutive relations and failure envelope for a plain-weave graphite/epoxy

textile composite. The model is based upon the analysis of an RVE, which is subjected to force and moment resultants of classical laminate theory. Thus there is no assumption about the uniformity of an applied load or strain, as any load can be represented by a combination of force and moment resultants. The micro-scale stresses within the RVE are computed using the finite element method. The relation between the average macrostress and macrostrains provides the constitutive relations for the material. Thus constitutive characterization matrices [A], [B], [D] are found directly from micromechanics. The microstresses are also used to predict the failure of the yarn or matrix, which in turn translates to failure of the textile composite. Using the DMM, the failure envelope is developed for in-plane force resultants, with and without applied moment resultants. No currently accepted failure criteria exist that may be used explicitly for the analysis of textile composites. Thus the methods and results employed herein are used to develop phenomenological failure criteria for textile composites. The results are compared to conventional methods that are not specifically developed for the analysis of textile composites, as a basis for evaluation.

CHAPTER 2
APPROACH

Micromechanical finite element analysis is performed to determine the constitutive relations and failure envelope for a plain-weave graphite/epoxy textile composite. The model is based upon the analysis of an RVE, which is subjected to force and moment resultants of classical laminate theory. Thus there is no assumption about the uniformity of an applied load or strain, as any load can be represented by a combination of force and moment resultants. The micro-scale stresses within the RVE are computed using the finite element method. The relation between the average macrostress and macrostrains provides the constitutive relations for the material. Thus constitutive characterization matrices [*A*], [*B*], [*D*] are found directly from micromechanics. The microstresses are also used to predict the failure of the yarn or matrix, which in turn translates to failure of the textile composite.

Finite Element Micromechanical Method

In the current study, stress gradient effects are investigated, and it is assumed that the stress state is not uniform across the RVE. This represents an extension of the micromechanical models used to predict the strength of textile composites [28-32]. The stress state is defined in terms of the well-known laminate theory load matrices [*N*] and [*M*] which describe force and moment resultants. Furthermore, structural stiffness coefficients analogous to the [*A*], [*B*], [*D*] matrices are defined. In this approach, these structural stiffness coefficients are computed directly from the micromechanical models, rather than making estimations based upon the homogeneous Young's modulus and plate

thickness. Accordingly, individual unit strains and unit curvatures can be applied to the micromechanical finite element model, and the resulting deformations are used to define the stiffness coefficient matrices. Conventional models essentially neglect the presence of [*M*] terms that result from non-uniformity or gradients in applied force resultants, thus assuming a uniform stress state for which only the [*N*] matrix is populated. The additional analysis of the [*M*] term includes information about the distribution, or gradient, of a non-uniform load. This can greatly increase the ability of a failure model to accurately predict failure for load cases in which such effects may well be predominant, such as in thin plates, concentrated loading, or impact loading.

The significance of including the analysis of moment terms is further illustrated in Figure 2-1. The moment term describes the *distribution,* not only the *magnitude*, of applied loading. Depending on the stress state of an RVE, an analysis incorporating stress gradient effects and inclusion of the consideration of applied moment could be of critical importance. In Figure 2-1a, the force resultant (*N*) is non-zero, but the uniform loading results in zero moment resultant (*M*). However, in load cases such as Figure 2-1b and 2-1c, the non-uniformity of applied loading leads directly to an appreciable moment term, which must be included in the analysis. In fact, in some cases it is possible that the net force resultant is zero while the effective moment resultant is non-zero, in which case conventional analysis techniques cannot be employed.

The present micromechanical analysis of a plain-weave textile composite is performed by analyzing the representative volume element (RVE) using the finite element method. A typical weave-architecture has been selected and this RVE is detailed in Table 2-1 and also in Figure 2-2. This architecture was chosen from a literature source

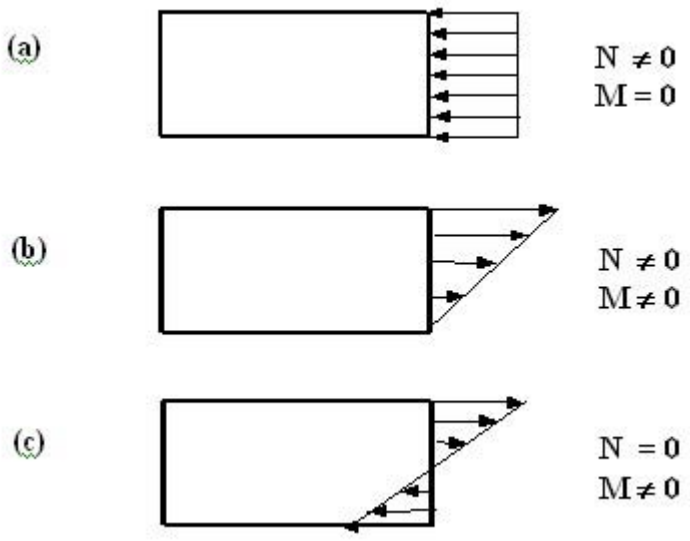

Figure 2-1. Example Load Cases to Illustrate the Importance of Including Moment Terms in the Analysis of a Textile RVE. Distributed Loads across the Large Dimensions of a Textile RVE Will Produce Bending Moments That Must Be Incorporated into Stiffness and Strength Prediction.

[33] that provided a complete and detailed description of the needed geometrical parameters, such as those shown in Table 2-1. Given parameters are representative of microarchitectures as experimentally observed via SEM or standard microscope.

Total fiber volume fraction, given these dimensions, will be 25%, incorporating the fact that the resin-impregnated tow itself has a fiber volume fraction of 65% (this is calculated directly from ABAQUS software, which yields element volumes as outputs, thus the volume of all matrix elements can be compared to the volume of all tow elements). Though this volume fraction may seem low for structural uses, it can be representative of many significant low-load, impact-resistant applications, such as automotive lightweight body panels.

Table 2-1: RVE Dimensions

Dimension	***a , b***	***c***	***p***	***t***	***w***
Length (mm)	1.68	0.254	0.84	0.066	0.70

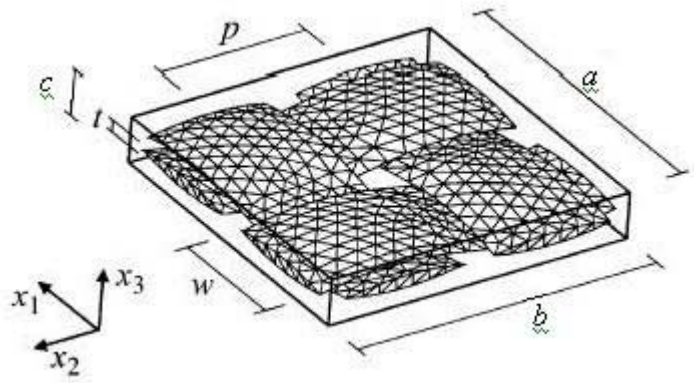

Figure 2-2: RVE Geometry of a Plain Weave Textile Composite

It should be noted that a number of parameters are required to exactly specify the textile geometry. These specifications will have a significant effect on micromechanical modeling. Consequently, care should be taken when comparing the results of various studies that the textile geometries under comparison are truly equivalent.

In order to evaluate the stiffness and strength properties of the textile weave under consideration, the DMM is essentially employed as an analytical "laboratory" that quickly and effectively replaces physical testing and experimental procedures. Though experimental verification always provides a baseline of veracity to FEM analysis, this procedure effectively overcomes the limitations of physical apparatus. Furthermore, as will be shown later, this allows for a dense population of analysis points; thus a failure envelope may be quickly and fully constructed with a large number of data points, and there is no need for interpolation of limited discrete experimental data points. Also, results achieved from the DMM are completely three-dimensional stress or strain fields. Thus, the results can be visualized throughout the thickness of the specimen. This overcomes the limitations inherent to physical application of experimental stress analysis techniques, which are labor-intensive and generally limited to surface visualizations.

Specification of relative displacements on opposite faces of the RVE can represent any general macro deformation under investigation. Displacements are applied using periodic boundary conditions. The periodic displacement boundary conditions isolate the mechanical effects of application of unit strains or curvatures, and ensure the repeatability of deformations. Thus, the RVE is not only repeatable as a representative geometry, but is also mechanically repeatable in that each RVE has an identical response to strains and curvatures regardless of the location of that RVE in a textile plate or component, for example

$$\left.\frac{\partial u_i}{\partial x_j}\right|_x = \left.\frac{\partial u_i}{\partial x_j}\right|_{x+a} \qquad \left.\frac{\partial^2 w}{\partial x^2}\right|_x = \left.\frac{\partial^2 w}{\partial x^2}\right|_{x+a} \tag{2.1}$$

To ensure continuity of microstresses and compatibility of displacements across an RVE, periodic traction and displacement boundary conditions must be employed. A macroscopically homogeneous deformation can be represented as

$$u_i^M = H_{ij} x_j \qquad \text{i,j = 1,2,3} \tag{2.2}$$

e.g. $u_i(a, x_2, x_3) - u_i(0, x_2, x_3) = H_{i1} a$

e.g. $u_i(x_1, b, x_3) - u_i(x_1, 0, x_3) = H_{i2} b$

The derivation of the periodic boundary condition for unit curvature is presented below, and further examples are presented in the appendix.

The periodic displacement boundary condition corresponding to unit curvature along the *x*-axis (κ_x) will be derived. All other curvatures will be zero. Curvatures are defined as follows

$$\kappa_x = -\frac{\partial^2 w}{\partial x^2} = 1 \quad \kappa_y = -\frac{\partial^2 w}{\partial y^2} = 0 \qquad \kappa_{xy} = -\frac{\partial^2 w}{\partial x \partial y} = 0 \tag{2.3}$$

The periodic displacement boundary condition will be derived from the definition of curvature along the *x*-axis (κ_x). Integrating once with respect to *x* yields

$$-\frac{\partial w}{\partial x} = x + f(y) \tag{2.4}$$

where $f(y)$ is an arbitrary function of *y*. Differentiation of this expression with respect to *y*, together with the requirement that κ_{xy} is set as zero, indicates that

$$\kappa_{xy} = -\frac{\partial^2 w}{\partial x \partial y} = f'(y) = 0 \tag{2.5}$$

Due to the above expression, *f(y)* must therefore be a constant, since $\kappa_{xy} = 0$. Furthermore, this constant must be zero due to the specification that slope at the origin is zero, such that $\left.\frac{\partial w}{\partial x}\right|_{x=0} = 0$ Next, Equation 2.4 is integrated with respect to *x*, giving rise to the following expression and an arbitrary function $h(y)$

$$-w = \frac{x^2}{2} + h(y) \tag{2.6}$$

Now coordinate values for opposite faces of the RVE (see Figure 2-2) may be substituted into Equation 2.6

$$\begin{aligned} w(a, y, z) &= -\tfrac{1}{2}a^2 + h(y) \\ w(0, y, z) &= h(y) \end{aligned} \tag{2.7}$$

These are then subtracted from each other, eliminating the unknown $h(y)$, and effectively prescribing the relative displacement on opposite faces that can be used to apply unit curvature.

$$w(a, y, z) - w(0, y, z) = -\tfrac{1}{2}a^2 \tag{2.8}$$

However, a further boundary condition is required to remove the transverse shear forces that will be present due to the application of this displacement. In this way, the mechanical effect of curvature is isolated. Thus the requirement is that transverse shear strain is zero, which is defined as

$$\gamma_{zx} = \frac{\partial u}{\partial z} + \frac{\partial w}{\partial x} = 0 \tag{2.9}$$

This can be rearranged as below, and the value of slope $\frac{\partial w}{\partial x}$ is known from Equation 2.4 above (where the arbitrary function has been shown to be zero).

$$\frac{\partial u}{\partial z} = -\frac{\partial w}{\partial x} = x \tag{2.10}$$

Similar to the above procedure, this expression can then be integrated with respect to z, evaluated with coordinate values of opposite faces, which are then subtracted from each other to specify the relative displacement that must be proscribed.

$$u = zx + c \tag{2.11}$$

$$u(a, y, z) - u(0, y, z) = za \tag{2.12}$$

The periodic boundary conditions as shown in Equations 2.8 and 2.12 must be simultaneously applied to isolate the effects of an applied unit-curvature.

In order to satisfy equilibrium, traction boundary conditions are applied to ensure equal and opposite forces on opposite faces of the RVE. The traction boundary conditions for traction forces on the lateral faces of the RVE are

$$\begin{aligned} F_i(a, y, z) &= -F_i(0, y, z) \\ F_i(x, b, z) &= -F_i(x, 0, z) \\ F_i(x, y, c) &= -F_i(x, y, 0) \end{aligned} \tag{2.13}$$

In the Direct Micromechanics Method (DMM), the RVE is subjected to macroscopic force and moment resultants, which are related to macroscopic strain and curvature according to

$$\begin{Bmatrix}[N]\\[M]\end{Bmatrix} = \begin{bmatrix}[A] & [B]\\[B] & [D]\end{bmatrix}\begin{Bmatrix}[\varepsilon]\\[\kappa]\end{Bmatrix} \tag{2.14}$$

Thus the constitutive matrices must be evaluated to determine this correlation. Once this has been determined, a macroscopic deformation can be applied using an FEM code. In this way, the FEM results for stress in each element yield the microstresses resulting from an applied force or moment resultant.

The RVE is subjected to independent macroscopic unit deformations in order to evaluate the stiffness matrices of Equation 2.14. In each of the six cases shown in Table 2-2 below, a single unit strain or unit curvature is applied, and all other deformation terms are set to zero, and the appropriate periodic boundary conditions are applied.

The four-node linear tetragonal elements in the commercial ABAQUS™ (Standard) FEM software package were used to model the yarn and matrix for all cases. An *h*-refinement convergence study was performed in which analysis was performed for a progressively finer mesh of four-node linear tetragonal elements. For several reasons, the final mesh chosen employs 68,730 such elements.

Table 2-2: Periodic Displacement Boundary Conditions

		u(a,y)-u(0,y)	***v(a,y)-v(0,y)***	***w(a,y)-w(0,y)***	***u(x,b)-u(x,0)***	***v(x,b)-v(x,0)***	***w(x,b)-w(x,0)***
1	$\varepsilon_x^M = 1$	*a*	*0*	*0*	*0*	*0*	*0*
2	$\varepsilon_y^M = 1$	*0*	*0*	*0*	*0*	*b*	*0*
3	$\gamma_{xy}^M = 1$	*0*	*a/2*	*0*	*b/2*	*0*	*0*
4	$\kappa_x^M = 1$	*az*	*0*	$-a^2/2$	*0*	*0*	*0*
5	$\kappa_y^M = 1$	*0*	*0*	*0*	*0*	*bz*	$-b^2/2$
6	$\kappa_{xy}^M = 1$	*0*	*az/2*	*-ay/2*	*bz/2*	*0*	*-bx/2*

This mesh refinement is significantly beyond the point of numerical convergence for which output element stresses can be assured to be accurate. This also allows for a mesh that accurately covers the "corners" of an ellipsoidal tow cross-section without sacrificing element quality in such regions. Furthermore, a refined mesh can capture the intricacies of stress contours and stress gradients expected to be seen through the RVE. Note that the shared nodes are employed between each tow and its surrounding interstitial matrix. There are no tow-tow shared nodes, thus tows are not bound to each other, but only to the interstitial matrix. As a final note on the character and quality of mesh employed in this analysis, the following quality assurance metrics are indicated: fewer than 0.1% of elements have an interior angle less than 20 degrees, fewer than 0.3% have an interior angle greater than 120 degrees, and less than 0.2% have an aspect ratio greater than 3 (the average aspect ratio is 1.66).

The FEM results for each element yield the microstresses resulting from an applied macro-level strain and curvature. The corresponding macro-level force and moment resultants in each case can be computed by averaging the microstresses over the entire volume of the RVE

$$N_{ij} = \left(1/_{ab}\right)\sum \sigma_{ij}^{e} V^{e} \tag{2.15}$$

$$M_{ij} = \left(1/_{ab}\right)\sum z\sigma_{ij}^{e} V^{e} \tag{2.16}$$

where e denotes summation over all elements in the FE model of the RVE, V^e is the volume of the e^{th} element, and a and b are the dimensions of the RVE as shown in Figure 2-2.

Thus the constitutive matrices of Equation 2.14 can be found by independently evaluating the six cases shown in Table 2-2, in tandem with Equations 2.15 and 2.16. By

applying the appropriate displacements according to Table 2-2 which correspond to a given unit strain or curvature case, the stiffness coefficients in a column corresponding to the non-zero strain can be evaluated directly from the force and moment resultant values as calculated from the finite element micro stresses via Equations 2.15 and 2.16. Thus the six load cases completely describe the six columns of the [*A*], [*B*], [*D*] matrix.

This information having been determined, one is then able to evaluate the microstress field resulting from general loading cases via the following steps: Step 1) Relate applied force and moment resultants to applied macro strain and curvature via the [*A*], [*B*], [*D*] matrices and Equation 2.14, Step 2) Apply this macro strain and curvature to the RVE using an FEM code, and Step 3) The element stresses from FEM results yield the microstress field in the yarn and matrix. The present study assumes there are no residual stresses or pre-stresses in the composite. The significance of residual stresses would depend on the particular cure cycle employed in manufacturing the composite, as well as upon the weave pattern under investigation. For a plain-weave textile, it would be expected that residual pre-stresses would affect the "center point" of the failure envelope, given that 1) symmetry of microarchitecture would lead to a level of symmetry of residual stresses, and 2) pre-stresses shift, rather than shrink, an existing failure envelope as the applied loads can either add to or be offset by the residual stresses. The magnitude of residual stresses could conceivably reach on the order of 10% of the failure strength.

Direct Micromechanics Method for Failure Analysis

The method described above can be used to predict strength by comparing the computed microstresses in each element against failure criteria for the constituent yarn and matrix of the textile composite. Interface failure is not considered in the current

study, but will be incorporated into future work. The microstresses in each element can be extrapolated from the preliminary RVE analysis (described above) of each of the six linearly independent macrostrain components. The microstress state for a general applied force or moment resultant is obtained by superposing multiples of the results from the unit macrostrain analysis

$$\left\{\sigma^{e}\right\} = [F^{e}]\begin{Bmatrix}\varepsilon^{M}\\ \kappa^{M}\end{Bmatrix} \tag{2.17}$$

Where the 6×6 matrix $[F^e]$ contains the microstress in each element resulting from the unit strain and curvature analysis. For example, the microstress σ_y in the RVE for ε_{x0} =0.05 and κ_y= 0.003 m^{-1} is calculated as $\sigma_y = 0.05F_{21}+0.003F_{25}$.

Failure is checked on an element-by-element basis, and the failure criterion of each element can be selected appropriately based upon whether it is a yarn or matrix element. It is assumed that the entire textile composite has failed, even if only one of the yarn or matrix elements has failed. Although this may be considered conservative, it is realistically representative of the initial failure of the composite.

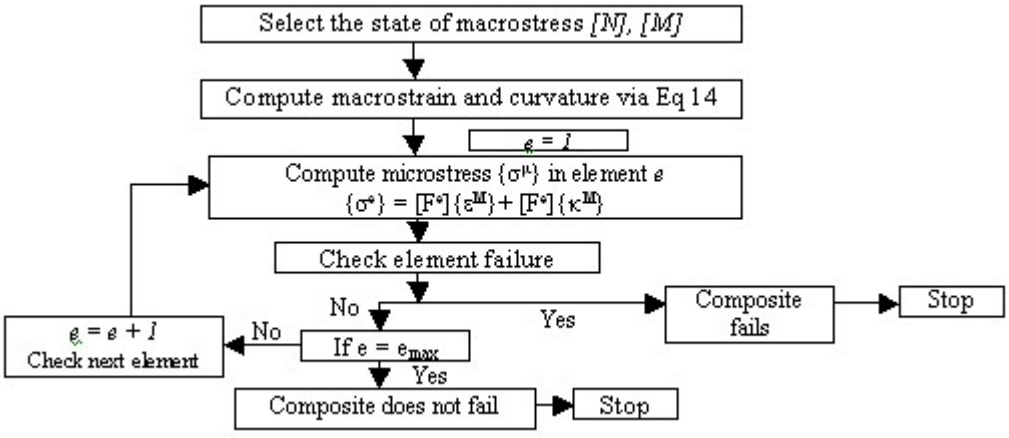

Figure 2-3: Flowchart for Failure Analysis Using the Direct Micromechanics Method

For the isotropic matrix elements, the Maximum Principal Stress criterion is used to evaluate element failure. For fiber tow elements, the Tsai-Wu failure criterion is used. This criterion is more suitable to the orthotropic nature of the fiber tow, which is essentially a unidirectional composite at the micro level. Microstresses in the yarn are transformed to local coordinates tangent to the path of the yarn and compared to strength coefficients for a unidirectional composite, using the Tsai-Wu criterion.

A flow chart that describes the DMM procedure is shown in Figure 2-3. Failure envelopes are generated by first selecting a macrostress state to investigate. Then the macrostrains and curvatures resulting from this applied loading are calculated from Equation 2.14. The resulting stress field for the entire RVE is then calculated by Equation 2.17, based on the scaled superposition of the results from FEM analysis of the unit load cases shown in Table 2-2. Failure is then checked in each element against a given failure criterion. This cycle is then repeated while progressively increasing a selected force or moment resultant and holding all others constant until an element level failure criterion is exceeded. If a particular failure criterion is exceeded, the element and the RVE are considered to have failed, which then defines the threshold of the failure envelope at a given point. Thus failure envelopes for the textile composite can be generated in various force and moment resultant spaces. The scope of the current study considers analysis of in-plane force and moment resultants [N] and [M], though the methods are applicable to any general loading conditions.

Phenomenological Failure Criteria

In addition to being used to determine failure of the fiber tow or the matrix phase at the element or micro level, the Tsai-Wu phenomenological failure criterion is used as a basis for comparison to the DMM for the macroscopic failure of the textile composite.

Since the Tsai-Wu criterion was formulated in terms of stresses, an adapted form of this criterion in terms of applied force resultants is used.

$$F_{11}N_x^2 + F_{22}N_y^2 + F_{66}N_{xy}^2 + 2F_{12}N_xN_y + F_1N_x + F_2N_y = 1 \tag{2.18}$$

Employment of this criterion essentially represents fitting an ellipse of Tsai-Wu form to the DMM failure data. The failure coefficients (F_{ij}) that appear in Equation 2.18 are based on failure data from the DMM. These parameters are based on the failure strength of the material under various loading conditions, and are typically determined by conducting physical tests on the specimen. For example, in order to obtain F_{11} and F_1, a load of N_x is applied, and all other stresses are set to zero. Then Equation 2.18 reduces to

$$F_{11}N_x^2 + F_1N_x = 1 \tag{2.19}$$

Since the DMM has been used to determine the maximum uniaxial tensile and compressive force resultant, each of which satisfy Equation 2.19, these two independent equations can be solved for F_{11} and F_1

$$F_1 = (1/X_T) - (1/X_C) \tag{2.20}$$

$$F_{11} = 1/(X_TX_C) \tag{2.21}$$

where X_T and X_C are the failure values of Nx for tension and compression, respectively. Using similar procedures, strength coefficients F_{22}, F_2, and F_{66} are evaluated. The resulting values are as follows

$$F_2 = (1/Y_T) - (1/Y_C) \tag{2.22}$$

$$F_{22} = 1/(Y_TY_C) \tag{2.23}$$

$$F_{66} = 1/S^2 \tag{2.24}$$

In the above equations Y and S are the strengths in terms of the force resultants N_y and N_{xy}, and C and T denote compression and tension, respectively. In the literature, there exist many proposed methods for determining an appropriate F_{12}. In this study, the coefficient F_{12} is determined by subjecting the unit-cell to a state of biaxial stress such that $N_x = N_y$ while $N_{xy}=0$, and then determining the maximum value of applied $N_x = N_y = N_{max}$. The resulting coefficient takes the following form

$$F_{12} = \frac{1}{2N_{max}^2}\left[1 - (F_{11} + F_{22})N_{max}^2 - (F_1 + F_2)N_{max}\right] \tag{2.25}$$

Please note that for Equations 2.18 through 2.25, strength values must be in terms of force resultants (N), as noted in the nomenclature. This is different from the textbook definition of the Tsai-Wu failure theory, which is in terms of stresses. Also note that, as will be discussed later, the Tsai-Wu failure theory includes no provision for the incorporation of applied moment resultants into the prediction of failure.

The Maximum Stress Theory is another failure theory to which the results of the DMM may be compared. Simply stated, failure occurs when any single stress component exceeds an allowable level.

$$\begin{aligned} &X_C < N_x < X_T \\ &Y_C < N_y < Y_T \\ &\left|N_{xy}\right| < S \end{aligned} \tag{2.26}$$

And similarly, the Maximum Strain failure theory states that failure occurs when any single mid-plane strain component exceeds an allowable level.

$$\begin{aligned} &e_C < \varepsilon_{x0} < e_T \\ &e_C < \varepsilon_{y0} < e_T \\ &\left|\gamma_{xy0}\right| < e_{LT} \end{aligned} \tag{2.27}$$

For example, the limiting mid-plane strain in a given direction is

$$e_i = \frac{N_{\max}/t}{E_i} \tag{2.28}$$

The bounds of the Maximum Strain Theory failure envelope take the shape of a parallelogram whose sides are defined by lines of the form

$$N_y = \nu_{xy} N_x + S_T \tag{2.29}$$

As was mentioned regarding the Tsai-Wu failure theory, the Maximum Stress and Maximum Strain theories were developed in terms of applied stresses, thus adapted forms of these criteria in terms of applied force resultants are used. Again, currently there is no provision for the incorporation of applied moments into the prediction of failure.

CHAPTER 3
STIFFNESS AND STRENGTH DETERMINATION

Using the DMM procedure as detailed in Chapter 2, the failure envelope for a plain weave textile composite is developed for in-plane force resultants, with and without applied moment resultants. No currently accepted failure criteria exist that may be used explicitly for the analysis of textile composites. Thus the methods and results employed herein are used to develop phenomenological failure criteria for textile composites. The results are compared to conventional failure envelopes that are not specifically developed for the analysis of textile composites, as a basis for evaluation.

Stiffness Properties

The fiber tow was assumed to have material properties of a unidirectional composite (weave geometry is taken into account in the finite element model), in this case AS/3501 graphite-epoxy.

The constitutive matrices relating macroscopic force and moment resultants to strains and curvatures were found using the aforementioned procedures and are found to be

$$[A] = \begin{bmatrix} 4.14 & 0.52 & 0 \\ 0.52 & 4.14 & 0 \\ 0 & 0 & 0.18 \end{bmatrix} \times 10^{6} (Pa - m) \qquad [B] \approx 0 \qquad (3.1)$$

$$[D] = \begin{bmatrix} 7.70 & 2.53 & 0 \\ 2.53 & 7.70 & 0 \\ 0 & 0 & 1.35 \end{bmatrix} \times 10^{-3} (Pa - m^{3})$$

The character of the constitutive matrices is analogous to an orthotropic stiffness matrix with identical elastic constants in the material principal directions (also referred to as a tetragonal stiffness matrix). Flexural stiffness values of the [*D*] matrix may seem slightly low, but it should be noted that the RVE under consideration is relatively thin at 0.254 mm. Also note that although the zero terms in the above matrices were not identically zero, they were several orders of magnitude below comparable matrix terms, and thus have been neglected with little or no effect on end results.

The above constitutive matrices have been calculated directly from the micromechanics model without any assumptions on the deformation of the composite such as plane sections remain plane etc. as in traditional plate theories. The results are quite different from commonly employed approximations. From classical laminate theory, a plane stiffness matrix is calculated from homogenized continuum stiffness properties (the familiar E, G, and ν). The flexural stiffness matrix [*D*] is then calculated from this homogenized stiffness and the thickness of the textile RVE. By comparison to the direct micromechanics results of the DMM, these methods will misrepresent flexural stiffness values D_{11}, D_{12}, and D_{66} by as much as factors of 2.9, 1.1, and 0.7 respectively. The DMM results imply that there is no consistent relation between in-plane and flexural properties, although the two properties are related.

In-plane axial and shear stiffness values (E, G) are calculated directly from the [*A*] matrix. Compared to the bare properties [34] of the constituent fiber tows (Table 3-1), stiffness is lower by an order of magnitude. But it must be noted that the textile composite under consideration here has on overall volume fraction of 25%, whereas the tow properties of Table 3-1 reflect the 65% volume fraction as seen within the tow itself.

As a basis for comparison, the in-plane homogenized stiffness properties are presented in Table 3-2, as calculated directly from the [*A*] and [*D*] matrices above. Flexural moduli, which represent the bending stiffness of the textile composite, are also presented in Table 3-2 and are calculated from the relations shown in Equation 3.2 through Equation 3.5.

$$E_{fx} = \frac{-M_x}{I_{yy}\kappa_x} = \frac{12}{t^3 D_{11}} \tag{3.2}$$

$$E_{fy} = \frac{12}{t^3 D_{22}} \tag{3.3}$$

$$G_{fxy} = \frac{12}{t^3 D_{66}} \tag{3.4}$$

$$\nu_{fxy} = \frac{D_{12}}{D_{11}} \tag{3.5}$$

Flexural moduli are material-dependent properties, but are strongly geometry-dependent as well. Similarly to what is seen for the in-plane stiffness, the flexural stiffness is shown to be much lower than the constituent tow properties, for the relatively thin plate under consideration here. The bending properties are strongly influenced by the plate thickness and the weave architecture.

Table 3-1: Fiber Tow and Matrix Material Properties

Material	E_1 (GPa)	E_2 (GPa)	G_{12} (GPa)	ν_{12}
AS/3501 Graphite/Epoxy (65% Fiber Volume)	138	9.0	6.9	0.30
3501 Matrix	3.5	3.5	1.3	0.35

Table 3-2: Stiffness Properties for Plain Weave Textile Plate

In-Plane Properties	$E_x = E_y$ (GPa)	G_{xy} (GPa)	ν_{xy}
	16.0	0.71	0.13
Flexural Properties	$E_{fx} = E_{fy}$ (GPa)	G_{fxy} (GPa)	ν_{fxy}
	5.0	0.88	0.33

Strength Properties

Table 3-3 [34] shows the textbook values for failure strengths of the yarn and matrix materials. The subscripts "L" and "T" refer to the longitudinal and transverse directions, respectively. The superscripts "+" and "-" refer to tensile and compressive strength. These were used with the Tsai-Wu failure criterion to determine failure of the yarn at the micro level within an element.

Figure 3-1 shows a comparison of the DMM failure envelope for the plain weave graphite/3501 textile composite with several common failure theories: the Tsai-Wu, Maximum Stress, and Maximum Strain failure theories. Failure envelopes are shown in the plane of biaxial force resultants with no applied moment present. Since the DMM is used to define the macro level failure strength, all theories share the same uniaxial strengths and are fit to these points.

For the most part, the Maximum Stress Theory is much more conservative than all other theories. However, it is less conservative in Quadrants II and IV, since this failure theory does not account for the interaction of biaxial stresses. The Maximum Strain and Tsai-Wu failure theories compare more closely to the DMM failure envelope, especially the latter.

For zero applied moment (Figure 3-1), the DMM failure envelope follows closely with the form of a Tsai-Wu failure envelope. For the most part, the initial failure mode is transverse failure of the fiber tows. However, at the extremes of the major axis of the

Table 3-3: Fiber Tow and Matrix Failure Strength Properties (MPa)

	$S_L^{(+)}$	$S_L^{(-)}$	$S_T^{(+)}$	$S_T^{(-)}$	S_{LT}
3501 / Graphite Tow	1448	1172	48.3	60	62.1
3501 Matrix	70	70	70	70	70

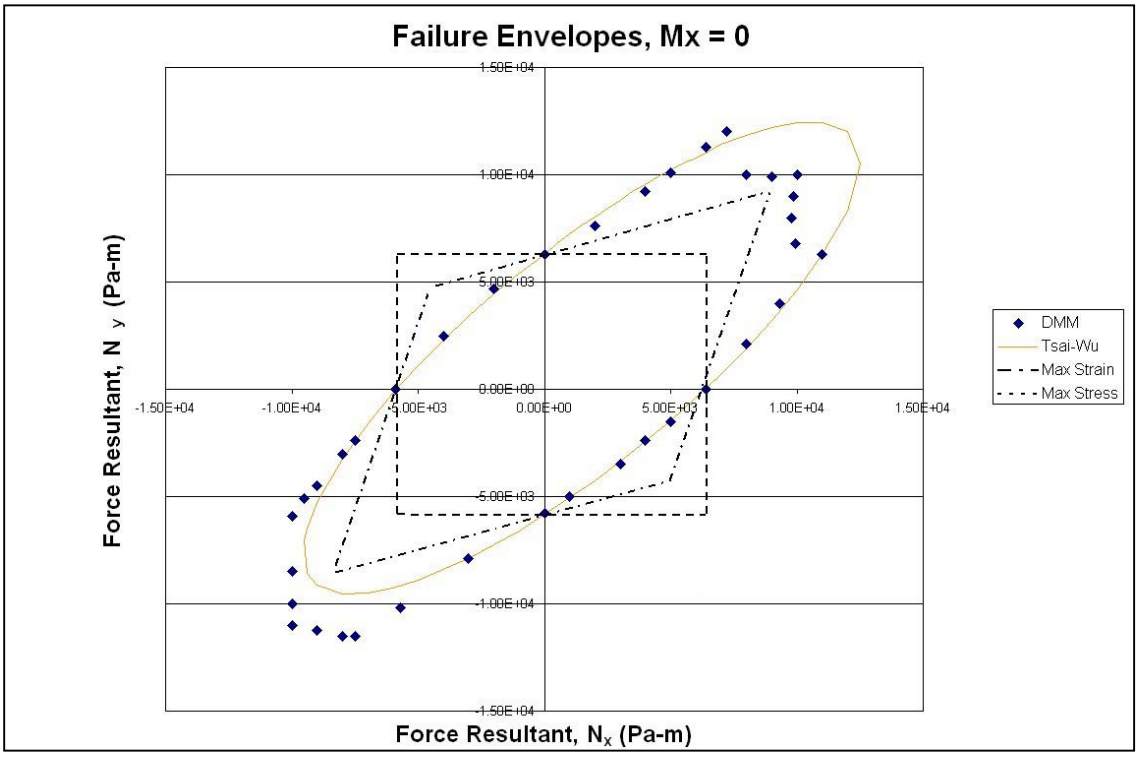

Figure 3-1: Comparison of DMM Failure Envelopes with Common Failure Theories. Adapted Forms of the Tsai-Wu, Maximum Strain, and Maximum Stress Failure Theories are Shown. Since the DMM is Used to Define the Macro Level Failure Strength, all Theories Share the Same Uniaxial Strengths and are Fit to these Points.

failure envelope (the outer corners of quadrants I and III), the initial failure mode transitions to failure of the matrix material. Thus the DMM failure envelope is cut short at the ends (compared to the failure envelope that would exist if matrix failure were not considered) and is squared-off in these regions and resembles the maximum failure stress (force resultant) criterion. The DMM envelope is more conservative than the Tsai-Wu type criterion in quadrant I, and slightly less conservative in quadrant III.

Though failure loads are not generally reported in terms of force and moment resultants, a translation of the failure envelope force resultant values to traditional stress values shows that strength magnitudes are reasonable based upon comparison to literature

and supplier-reported values for this material, geometry, and the relatively low fiber volume fraction (25%). Since the yarn takes much of the load, the matrix does not begin to fail until a much higher load than its bare tensile strength. Although the strength value is a fraction of the pure tow strength, the woven tow is not completely aligned in the loading directions. Some of the tow is curved into the thickness direction, thus providing through-thickness reinforcement. Furthermore, after initial transverse failure of the fiber tow (indicative of the introduction of intra-tow micro-cracking), the structure will still maintain load-bearing capacity, though stress concentrations will begin to build up and part integrity will be degraded. Also note that, due to symmetry of the textile RVE about the *x*- and *y*- axes, the failure envelope exhibits this symmetry as well.

The effect of an added moment M_x on the failure envelope is shown in Figure 3-2 with the applied moment M_x equal to half the critical value that would cause failure if it were the only applied load. The figure also includes results from Figure 3-1, the DMM results and quadratic failure envelope for the case of zero applied bending moment. There is no Tsai-Wu, Maximum Stress, or Maximum Strain failure envelope to include applied moment resultants, as these theories are not developed to include such load types. As has been mentioned, strength estimates will be somewhat conservative given that failure is defined as failure of a single element that surpasses the maximum allowable microstress, but this presents a realistic definition of initial failure.

Continuing to inspect Figure 3-2, an applied moment in the *x*-direction has the expectable effect of shrinking the failure envelope in regions where tensile applied loads dominate. However, when only compressive loads are applied, an applied moment can actually increase the in-plane load capacity by offsetting some of the compressive stress

with bending-induced tension. The magnitude of this load-capacity increase is limited, however, by the eventual failure of the matrix. As with the case of pure in-plane loading, the failure envelope at the outer corner of quadrant III is dominated by matrix failure. The effects of applied moment on the failure envelope of the plain weave textile represents the importance of the consideration of stress gradients, or load non-uniformities. The appreciable difference that arises suggests that such consideration could be critical to the successful design or optimization of a textile structural component.

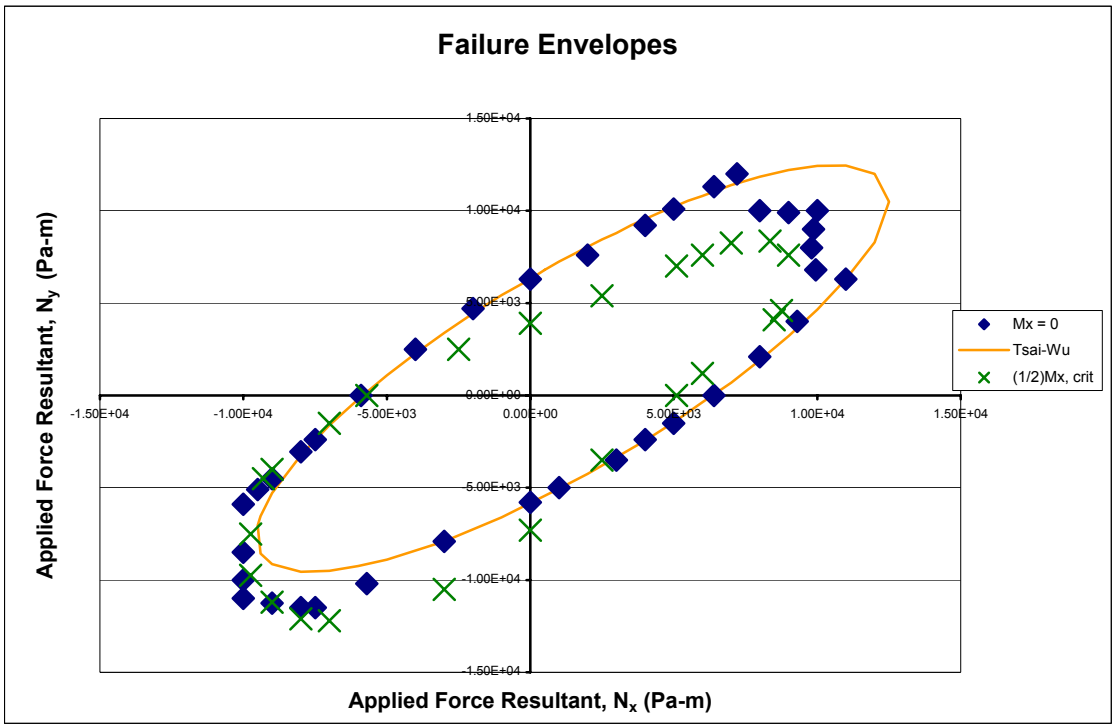

Figure 3-2: Effect of Bending Moment on the Failure Envelope. The Overall Envelope Decreases Significantly in Size. The Tsai-Wu Failure Ellipse is Unaltered when Moment is Applied, as the Theory Includes No Provision for this Load Type.

The effect of changing the failure theory used to define failure of a tow element at the micro (elemental) level is shown in Figure 3-3. The DMM can easily be modified to employ any appropriate failure criterion for the constituent phases at the

micromechanical level. Here, the Maximum Stress Failure Theory (MSFT) is used to replace the Tsai-Wu failure theory to determine first-element failure for the fiber tows. Though the overall character of the failure envelope is unchanged, the effect is quite significant in that the failure envelope becomes roughly half as conservative. It should be noted that, even in the case of simple uniaxial macro applied loads, the micro stress field that results is fully three-dimensional and non-homogeneous across the RVE. Thus, especially for the orthotropic fiber tows, a failure theory that includes multi-dimensional stress interaction effects (such as Tsai-Wu) should be more appropriate.

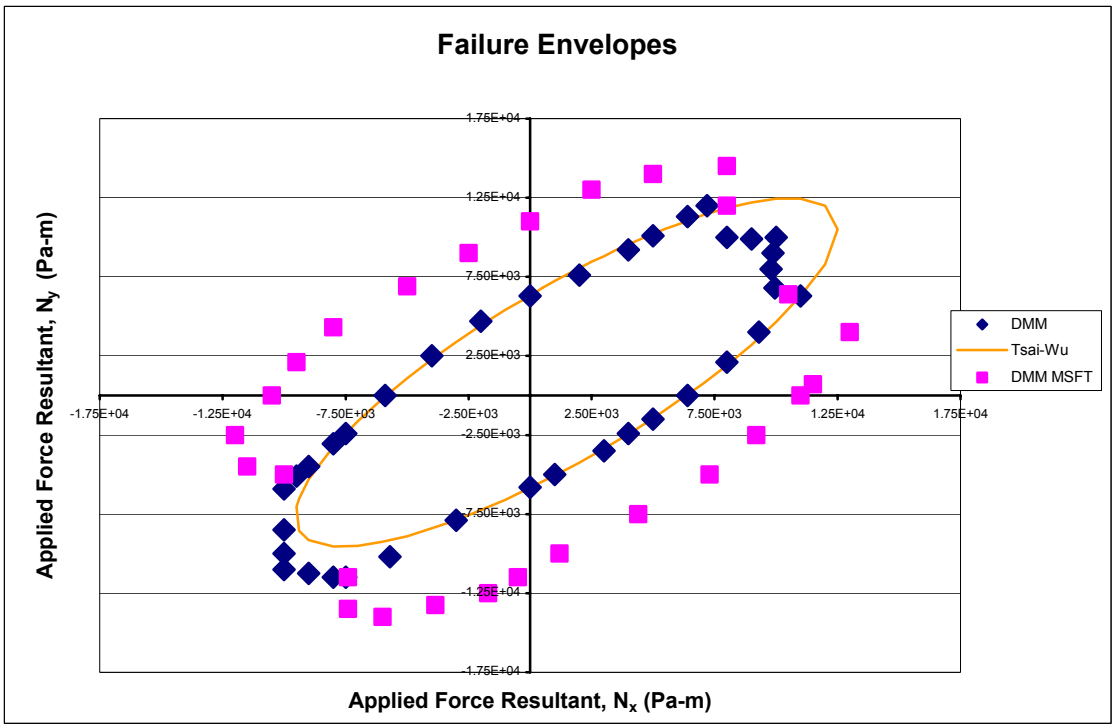

Figure 3-3: Effect of Micro-Level Tow Failure Theory on the DMM Failure Envelope. A Comparison is Shown between the Original DMM Using the Tsai-Wu Theory to Analyze Failure of a Tow Element and an Altered DMM in which the MSFT is Used

As mentioned earlier, we have assumed that the entire textile composite has failed, even if only one of the yarn or matrix elements has failed. It is possible to change the

definition of failure by stating that failure is considered to have occurred when 1% of the total number of elements have failed. Figure 3-4 shows the effect of changing the definition of failure and consequently the macro failure envelope. Note that failure points are shown in the plane of uniaxial applied force and moment resultants, in order to illustrate these effects under different loading types. About a 30% increase in maximum allowable force or moment resultant results from changing the definition of initial failure. This is shown to present the possibility of a more stochastic or a less conservative approach to determining the point at which initial failure occurs, thus only a few points are presented.

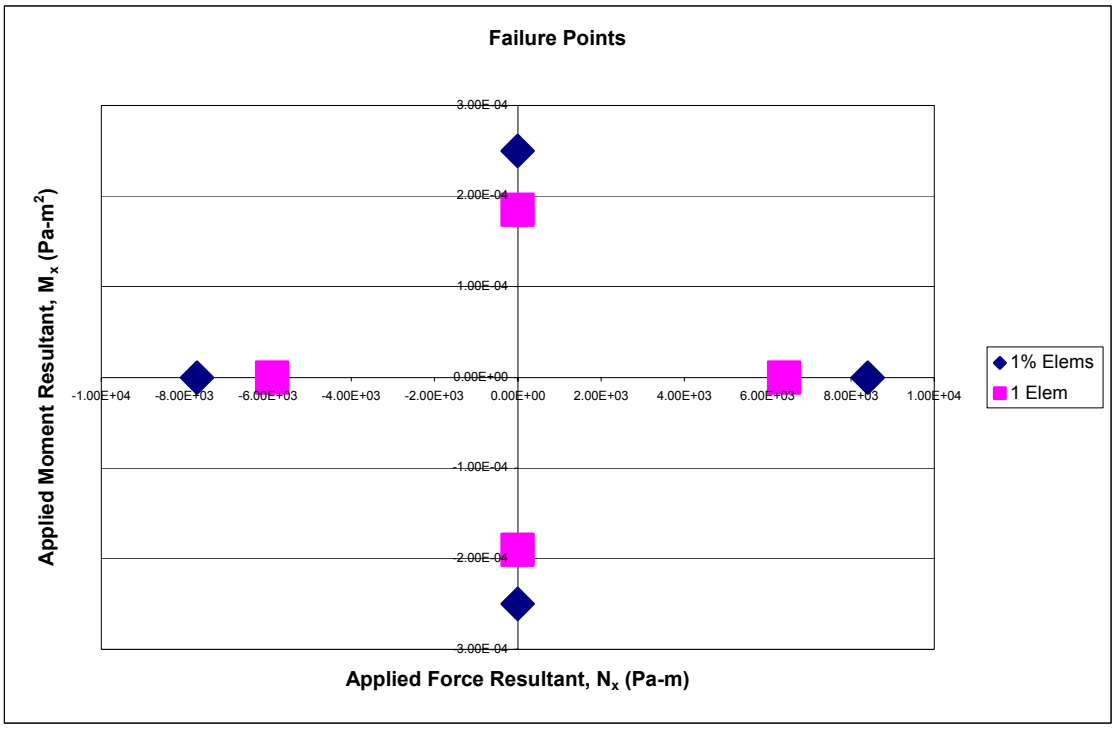

Figure 3-4: Effect of Changing the Definition of Micro-Level Failure on the Failure Envelope. The Allowable Force or Moment is Shown to Increase by 30% if Failure is Defined as the Point at which 1% of Elements Have Exceeded Failure Criterion, as Compared to the Point at which One Single Element Has Failed.

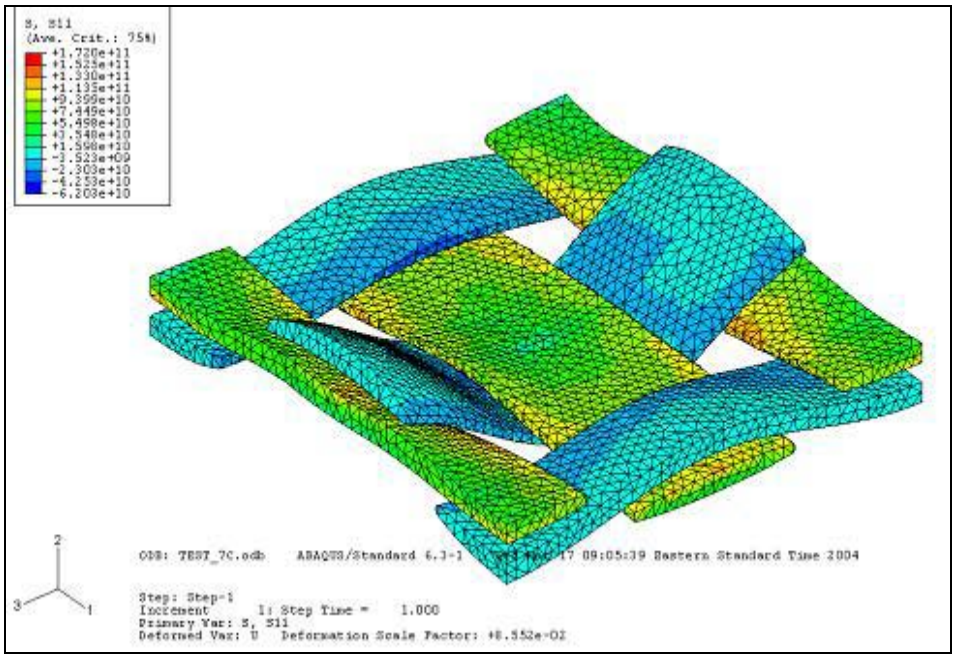

Figure 3-5: Stress Contours for Plain-Weave Fiber Tows in Uniaxial Extension. Detailed Microstress Field Results from the DMM Provide Valuable Insight into the Mechanical Response of an RVE under Any Loading Condition. Tow Elements or Matrix Elements Can Be Isolated to Provide Further Detail.

Microstress Field Contour Plots

Detailed stress-field contour plots are one output of the DMM that provide great insight into the failure modes and points of maximum stress in the RVE. Tow or matrix portions of the RVE can be isolated for individual scrutiny. Figure 3-5 shows the stress field for the plain-weave fiber tows in uniaxial tension. Most of the load in this case is taken by the fiber tows aligned in the loading direction. However, the failure mode is transverse failure of the cross-axis tows, as the strength is much lower in this direction. Tows aligned in the direction of loading tend to be pulled straight as load is applied. This has the secondary effect of applying bending to the cross-axis tows, creating significant bending stresses. The maximum stress levels in this micro stress field tend to occur around the matrix pockets between tows, which tend to act as a micromechanical stress concentration. Similar inspection of the stress field in the matrix surrounding the fiber

tows (not shown here) shows that the maximum stress tends to occur along the relatively sharp edges of the lenticular fiber tows, which again tend to act as a micromechanical geometrical stress concentration.

Further stress contour plots illustrating results and capabilities of the DMM show the RVE behavior in shear and bending load cases. For unit bending load cases, it is shown that the majority of the load is again taken by the fiber tows along the direction of curvature. Furthermore, just as there is a transition from tension to compression across the RVE in bending, a rapid stress gradient from tension to compression can be seen in an individual fiber tow. This again suggests the importance of the consideration of stress gradients in the micromechanical characterization of a textile RVE.

Inspection of Failure Envelopes in Additional Stress Spaces

Based on an extension of the results presented also in [28] and shown earlier in Figure 3-2, failure envelopes in the space of N_x - N_y - M_x (a practical and useful failure space which illustrates the limits of biaxial loading and the importance of consideration of stress gradients across an RVE) are seen to be characteristically elliptical in nature. This is due to the prevalence of stress interaction effects, as well as the symmetry of the plain weave geometry under analysis.

Figure 3-6 shows the discrete failure points as determined from the DMM for cases of biaxial loading with constant applied moments of 0, 0.3, 0.5, and 0.8 times the critical moment that would cause failure if it were the only load present. Phenomenologically, it can be seen that the failure envelopes become smaller as a larger moment (stress gradient) is applied. An applied moment has the expectable effect of shrinking the failure envelope, though in limited regions it has been seen that the complexity of the superposed stress fields may have an offsetting or beneficial effect.

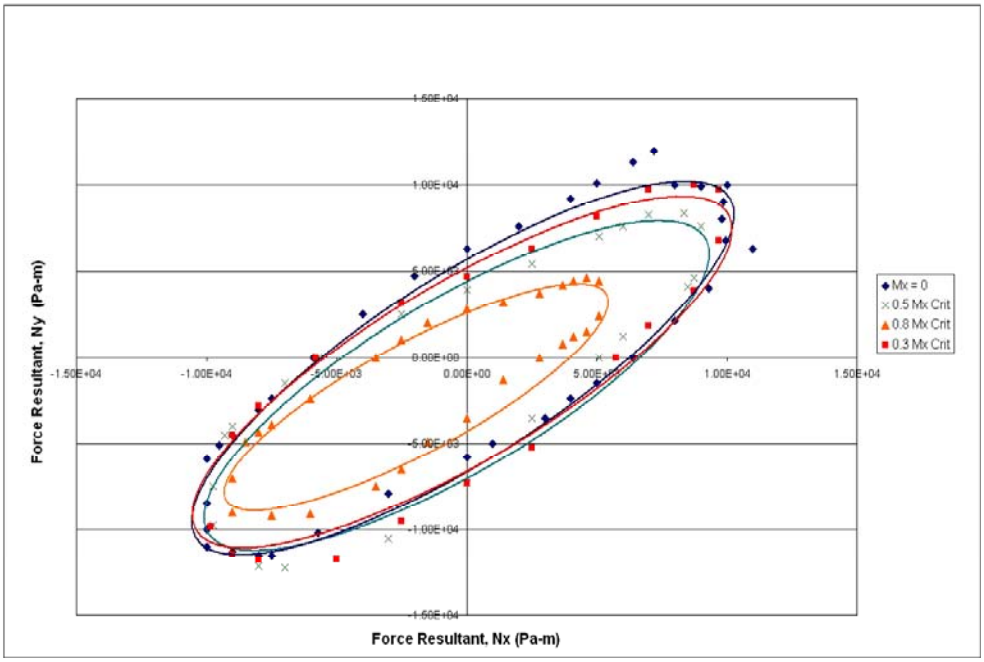

Figure 3-6: DMM Failure Envelopes for Biaxial Loading with Multiple Constant Moment Resultants. For Illustration, an Ellipse is Fit to Each Data Set Using a Least-Squares Method.

Also shown in this figure are elliptical fits to each failure envelope, which were computed by a Matlab™ based routine that was used to determine a least squares fit to the DMM data points. Regular analytical trends in these failure envelopes lead directly to the development of failure prediction methods which will be detailed in Chapter 4.

In general, failure envelopes in spaces other than those shown in Figure 3-6 will not necessarily be elliptical in nature, as has been observed for cases including shear, twist, and multiple moment loading terms. Figures 3-7 and 3-8 show failure envelopes in spaces of M_x - M_y - M_{xy} and N_x - M_x - N_{xy} respectively. Discrete points represent the failure envelopes as determined by the DMM.

Figure 3-7 isolates the relative effect of moment resultants, or stress gradients, of varying types on the failure envelope, as well as the interaction of multiple moments. Each envelope is mapped out with a constant applied twist M_{xy}.

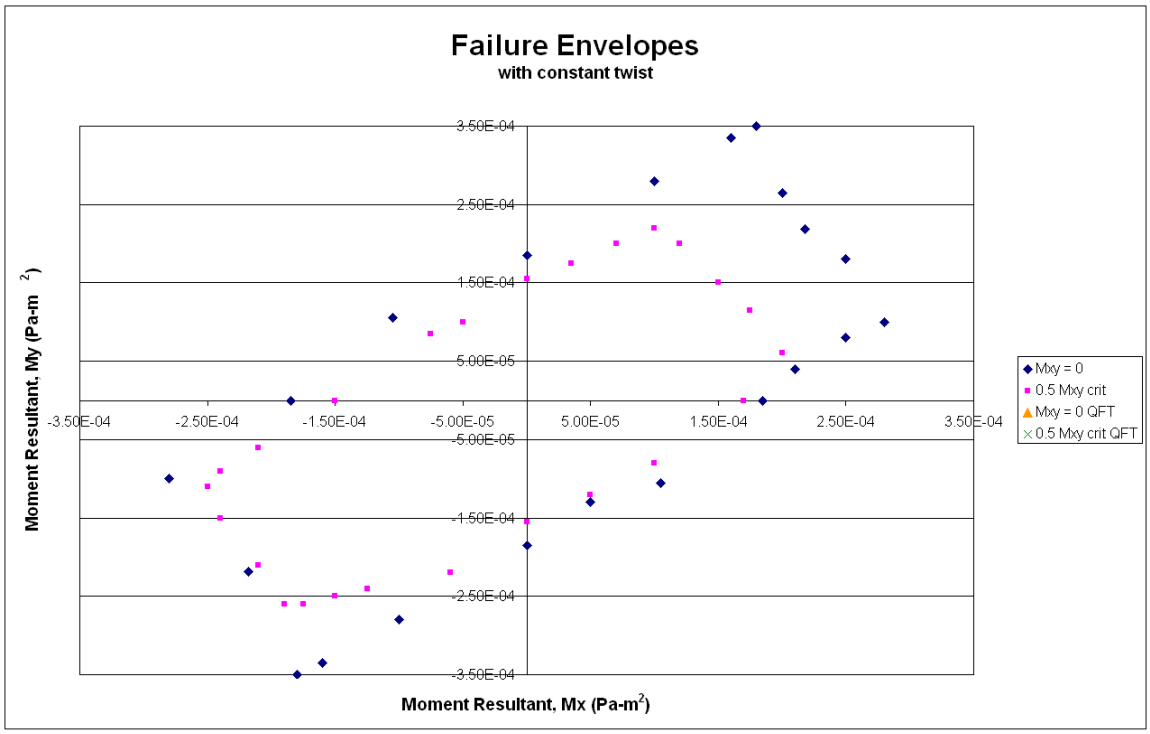

Figure 3-7: DMM Failure Envelopes for Biaxial Bending with Constant Applied Twisting Moment.

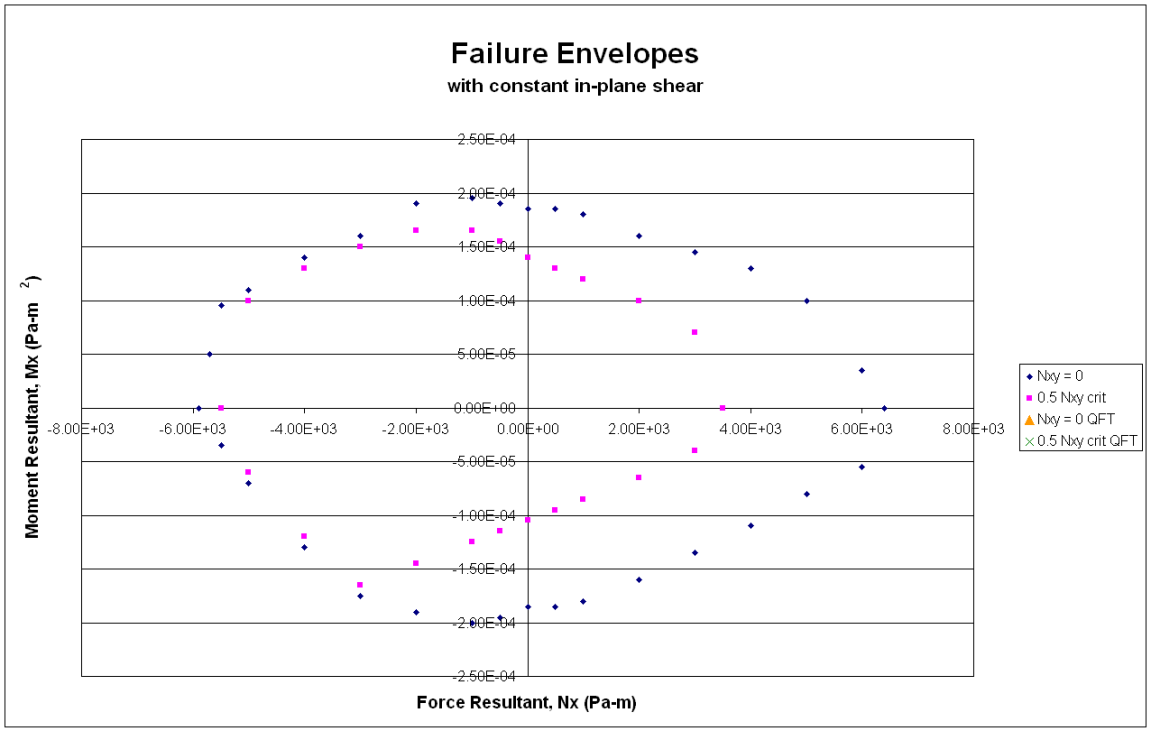

Figure 3-8: DMM Failure Envelopes with Force and Moment Resultants for Constant Applied Shear.

The overall character of Figure 3-7 is in some ways similar to that of Figure 3-6, in that the failure envelope symmetry reflects the symmetry of geometry and loading. Further, the strength limits in quadrants II and IV are lower due to stress interactions. Whereas for biaxial loading, strength is decreased when stresses act in the direction of the natural tendency of Poisson effects, in bending the strength is decreased when biaxial bending acts in the direction of the natural tendency of anticlastic curvature. As is generally seen in all failure analyses that have been performed in this study, the dominant mode of failure is transverse failure of the fiber tow.

The N_x - M_x - N_{xy} failure envelope (Figure 3-8) provides a visualization of the effect of the magnitude of stress gradient, or loading non-uniformity, for a given force resultant. Each envelope is drawn for constant in-plane shear to further incorporate the effects of multiple loading types. The envelope is symmetric about the *x*-axis due to the mechanical equality of positive or negative bending moment. This symmetry is not seen about the *y*-axis since the carbon-epoxy plain weave responds differently when in tension or compression.

Design of Experimental Verification

A procedure is suggested here which may be used to illustrate the differences between DMM and conventional failure points (a point which will also be visited in Chapter 5). Figure 3-9 shows a schematic representation of an off-axis test specimen. This specimen can be used under uniaxial tension to investigate different stress states. The orientation angle (θ) represents the angle of the principal material axes of the plain-weave with respect to specimen bounds.

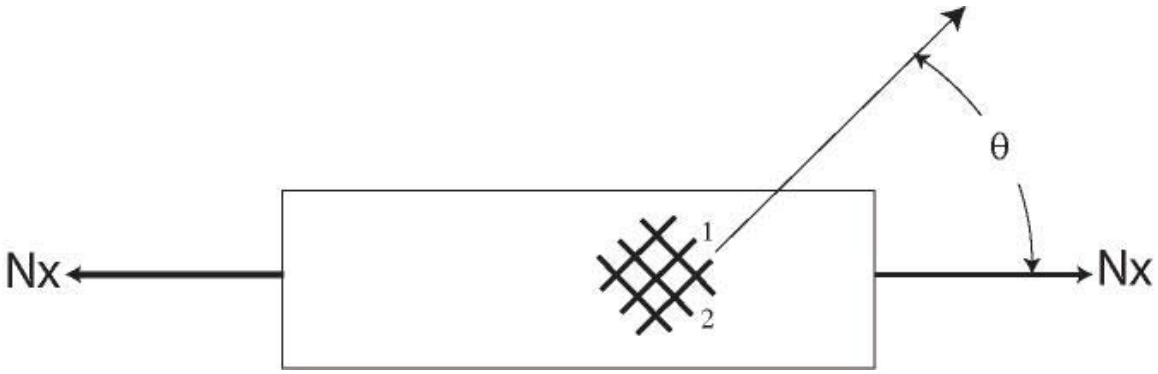

Figure 3-9: Schematic of the Specimen for Off-Axis Uniaxial Testing.

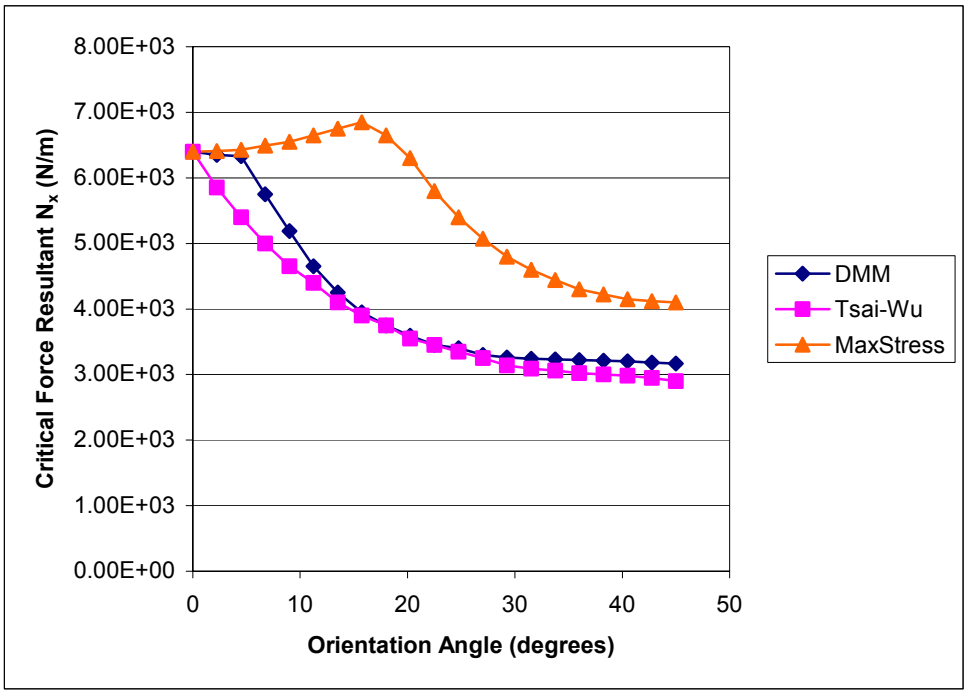

Figure 3-10: Critical Force Resultant under Uniaxial Loading as Calculated via Various Failure Theories.

Figure 3-10 shows a comparison of the maximum allowable force resultant N_x that may be applied, as calculated via the DMM, Tsai-Wu Failure Theory, and the Maximum Stress Theory, for various orientation angles. Data collected for tests performed at 0.08 radians (4.5 degrees) will produce data that should illustrate the greatest disparity

between DMM and the Tsai-Wu Failure Theory. At this point, the DMM predicts a failure load 17% less conservative than Tsai-Wu. Thus this can serve as an effective illustration to compare and contrast the two theories. Similarly, tests performed for a 0.31 radians (17.8 degrees) specimen will provide a comparison point most useful to investigate differences between predictions from DMM vs. Max Stress failure theories. At this point, the DMM predicts failure levels 32% more conservative.

Chapter Summary

By analysis of the microstresses developed in a representative volume element (RVE), the Direct Micromechanics Method (DMM) has been used to construct failure envelopes for a plain weave carbon/epoxy textile composite in plane stress. To allow for the accommodation of stress gradients, or non-uniform applied loads, micromechanical analysis had been performed in terms of classical laminate theory force and moment resultants [N], [M] and constitutive matrices [A], [B], [D]. The predicted values of the stiffness matrices and ultimate strength values compare well to expectable magnitudes. The DMM failure envelope was shown to be largely elliptical of the form of a Tsai-Wu failure criterion and dominated by transverse fiber tow failure. But in cases of large biaxial tension or biaxial compression loads, the DMM failure envelope compared to the form of the Maximum Stress Criterion, and matrix failure was the mode of initial failure. The presence of applied moment resultants [M], as would exist in cases of non-uniform load across the RVE, was shown to have a significant effect on the failure envelope. Thus its consideration, not covered in conventional failure models, can be critical.

The diversity of the failure spaces seen here is a harbinger of the further need to develop analytical methods to predict failure without pre-knowledge of the nature of the failure envelope. This will be discussed in Chapter 4.

CHAPTER 4
PREDICTION OF FAILURE ENVELOPES

The current chapter presents methods for utilizing the results presented in Chapter 3 to develop a failure criterion for textile composites. Using the DMM, the failure envelope is developed for in-plane force resultants, with and without moment resultants. No currently accepted failure criteria exist that may be used explicitly for the analysis of textile composites, or which include this ability to account for stress gradients at the micromechanical level. Thus the methods and results employed herein are used to develop phenomenological failure criteria for textile composites. Based on the DMM results, two methods are presented which may be used to predict failure of a textile composite. The first is a parametric method based on prediction of regular trends in the failure envelopes of a given 3D stress space. The second method represents the formulation of a 27-term quadratic failure equation that can be evaluated to determine failure of the textile under any general force and moment resultants.

A Parametric Approach to Predicting Failure Envelopes for a Given Stress Space

Referring again to the results of Figure 3-6, the observation is repeated that, phenomenologically, the failure envelopes become smaller as a larger moment (stress gradient) is applied. An applied moment has the expectable effect of shrinking the failure envelope, though in limited regions it has been seen that the complexity of the superposed stress fields may have an offsetting or beneficial effect.

Analytically, it can be seen that there are definite trends in the axes and placement of the failure ellipses. Failure ellipses were then characterized with parameters such as

major axis length, minor axis length, ellipse axis orientation angle, and the ellipse center point. Any general ellipse in (x, y) space can be represented by the expression

$$\left[\frac{x\cos\theta + y\sin\theta - u_0}{a}\right]^2 + \left[\frac{-x\sin\theta + y\cos\theta - v_0}{b}\right]^2 = 1 \qquad (4.1)$$

where θ is the orientation angle of the major axis of the ellipse with respect to the x-axis, u_o and v_o are the coordinates of the ellipse center point, a is half the major axis length, and b is half the minor axis length. For each failure ellipse shown in Figure 3-6, these parameters were then plotted as functions of the moment applied for each case, in order to inspect parametric trends.

For example, Figures 4-1 and 4-2 show the major and minor axis length of several N_x - N_y - M_x failure envelopes plotted against the moment resultant M_x applied in each case. A limited number of fitting cases were used, in order to reserve an adequate number of test cases and to prevent over-fitting of the trends.

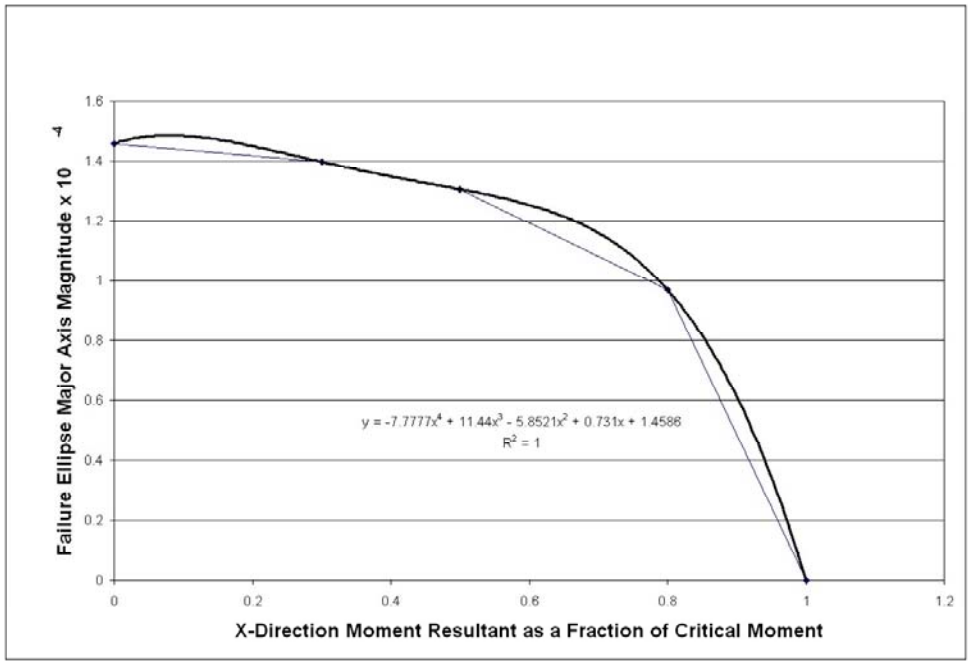

Figure 4-1: Effect of Applied Moment Resultant on the Major Axis of Elliptical Failure Envelopes.

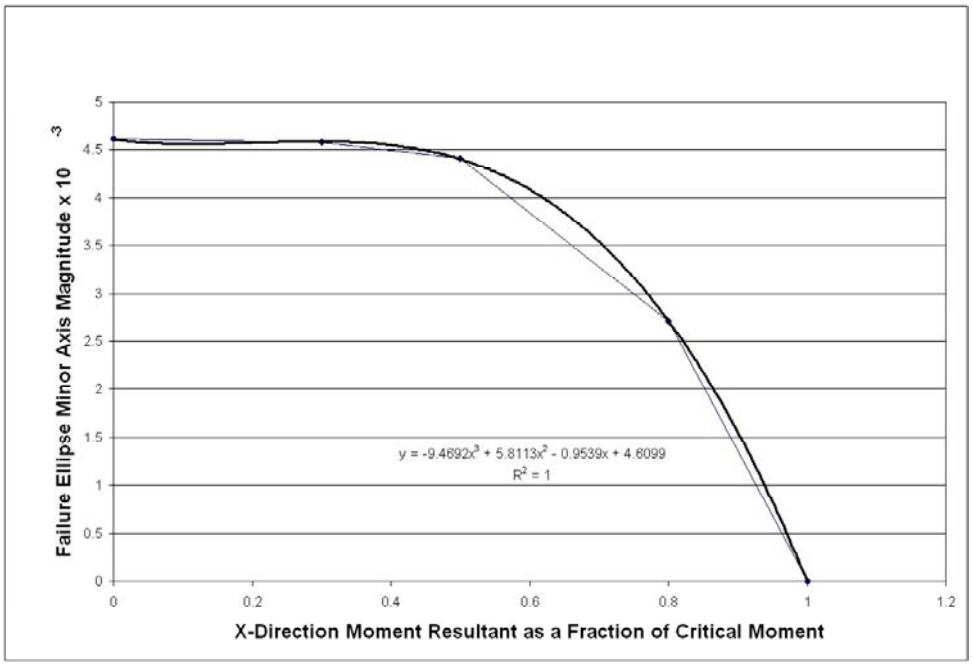

Figure 4-2: Effect of Applied Moment Resultant on the Minor Axis of Elliptical Failure Envelopes.

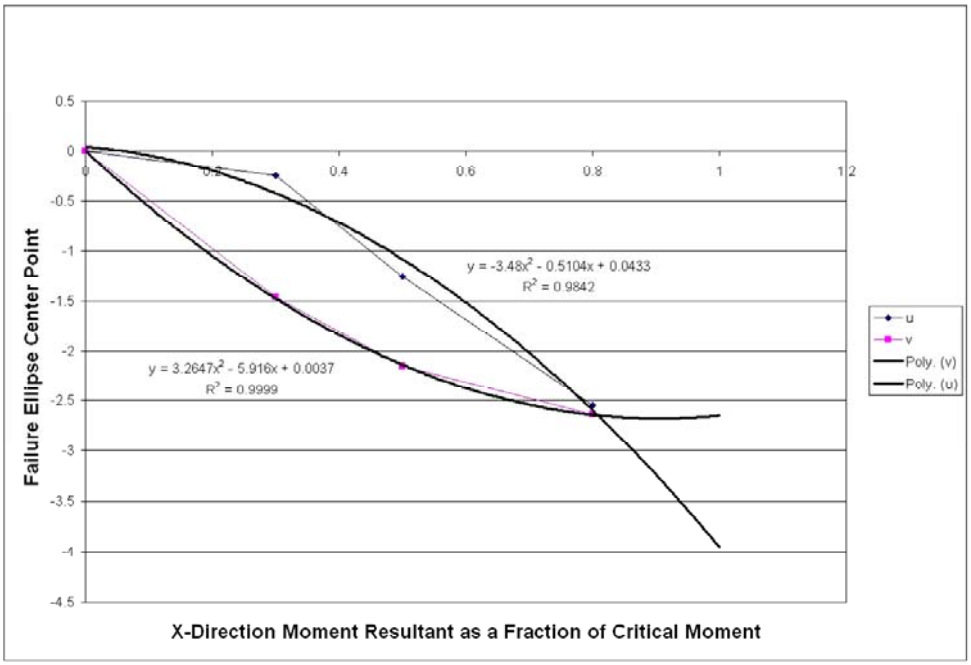

Figure 4-3: Effect of Applied Moment Resultant on the Center Point Coordinates (u_o , v_o) of Elliptical Failure Envelopes.

As mentioned earlier and as seen in these above figures, a larger applied moment with a given failure envelope has the effect of shrinking the envelope's major and minor

axes. These trends were regular enough to be closely approximated with a polynomial trend line. At the critical moment, the ellipse axes lengths become zero, as a load sufficient for failure is already applied, and no additional force resultants may be applied.

In addition to shrinking the failure envelope, larger applied moments also tend to cause a small but significant shift in the center point of the failure ellipse. This is caused by the fact that an applied moment is still a directional loading, and thus produces a directional bias in the location of the failure envelope. These trends were also plotted (Figure 4-3) and approximated with polynomial trend lines. Ellipse orientation angle (θ) was found to be nearly constant, thus no trend plot is shown.

Based on the above, an elliptical failure envelope of the form of Equation 4.1 can be predicted by evaluating the expressions for ellipse parameters in terms of applied moment resultant, as shown below

$$\left[\frac{N_x \cos\theta + N_y \sin\theta - u_0}{a}\right]^2 + \left[\frac{-N_x \sin\theta + N_y \cos\theta - v_0}{b}\right]^2 = 1 \qquad (4.2)$$

$$M = \frac{M_{applied}}{M_{critical}}$$

$$a = -7.77M^4 + 11.44M^3 - 5.85M^2 + 0.73M + 1.4586$$

$$b = -9.47M^3 + 5.81M^2 - 0.95M + 4.6 \qquad (4.3)$$

$$u_0 = -3.48M^2 - 0.51M$$

$$v_0 = 3.26M^2 - 5.92M$$

Thus any general N_x - N_y - M_x failure envelope can be predicted with the above procedure and expressions. For several test cases, a failure ellipse is predicted and

compared to discrete failure points as calculated directly from the DMM. These comparisons are shown in Figure 4-4 and Figure 4-5. The average deviation between the failure envelope predicted from the parametric curve fitting as compared with the direct results of micromechanical modeling was less than 2%.

The greatest value of this parametric approach to predicting failure is that it provides good insight into the exact nature of the failure space under consideration. Further, the results are quite accurate and could be useful for design purposes. However, the load cases are limited, and the methods presented here would have to be extended if more than three simultaneous loads were to be applied and analyzed.

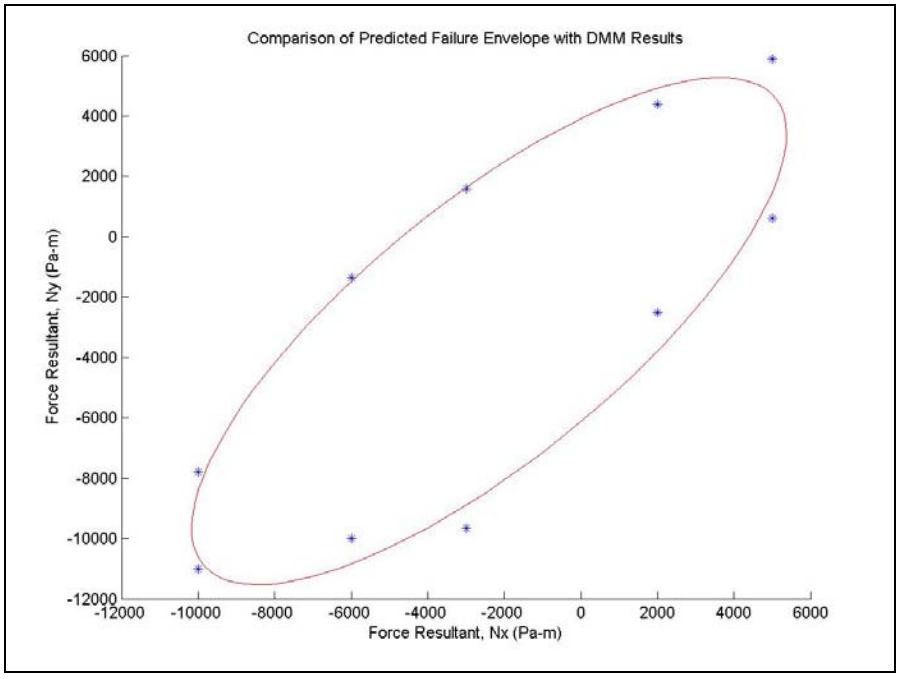

Figure 4-4: Failure Envelopes Predicted with the Parametric Approach as Compared to DMM Results (Applied Moment Resultant of 0.65 Critical Moment)

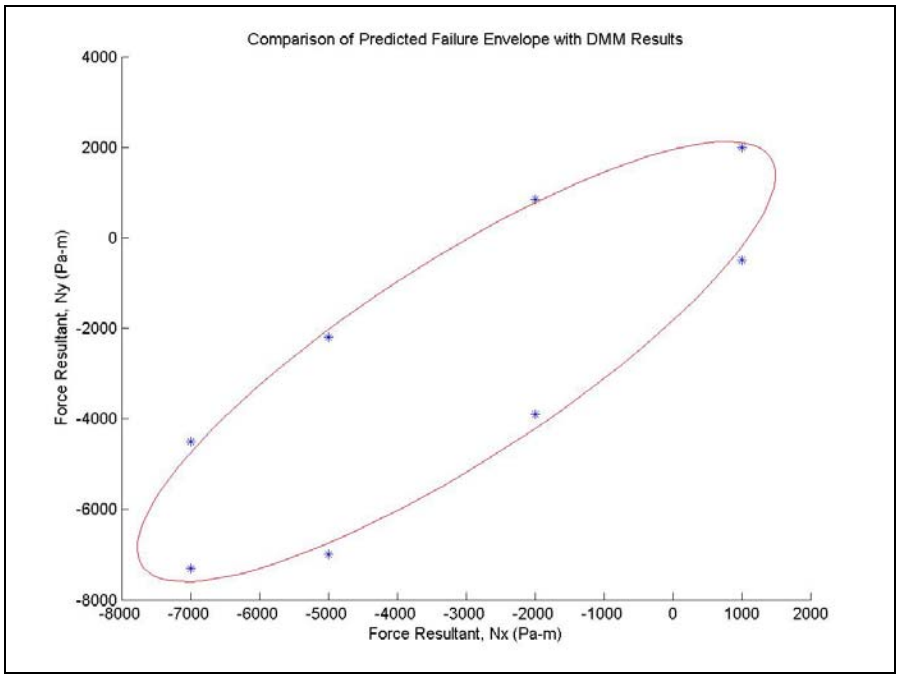

Figure 4-5: Failure Envelopes Predicted with the Parametric Approach as Compared to DMM Results (Applied Moment Resultant of 0.9 Critical Moment)

Development of a Quadratic Failure Criterion to Predict Failure for General Loading

In order to bind together the failure spaces, which can be quite different in nature, as can be seen in Figure 3-6 through Figure 3-8, methods of the previous section will not be readily applicable. Therefore, development of an additional analytical method becomes necessary. Further, an analytical approach to binding the results of multiple failure envelopes as calculated via the DMM, along with the capacity to accommodate any general plate loading condition has a practical value. Given the quadratic interactive nature of the stress state in determination of failure, an expression of the below form has been developed to predict failure.

$$C_{ij}F_iF_j + D_iF_i = 1 \tag{4.4}$$

where F_i represent general load terms ($N_x\, N_y\, N_{xy}\, M_x\, M_y\, M_{xy}$) , and C_{ij} or D_i represent 27 failure coefficients such that Equation 4.4 defines failure when its magnitude exceeds 1.

Failure coefficients C_{ij} and D_i can be solved given a sufficient amount of known failure points or failure envelopes. However, Equation 4.4 is numerically ill-conditioned given the great disparity in the magnitude of N_{ij} and M_{ij} loads which will cause failure. These values will differ by many orders of magnitude when typical units are utilized (Pa-m and Pa-m^2). This makes accurate solution of failure coefficients impossible when both such load types are present. Thus, Equation 4.4 must be defined in terms of F_i terms that are normalized with respect to a critical N_{max} or M_{max} that would cause failure if it were the only load present.

Coefficients C_{ii} and D_i can be solved by evaluating Equation 4.4 with a load of F_i and setting all other loads at zero. For example, in order to obtain C_{11} and D_1 a load of $F_1 = N_x$ is applied, all others are set to zero, and Equation 4.4 reduces to

$$C_{11}N_x^2 + D_1N_x = 1 \tag{4.5}$$

Since the DMM has been used to determine the maximum tensile and compressive allowable N_x, each of which must satisfy Equation 4.5, two independent equations are generated which can be simultaneously solved to yield C_{11} and D_1. Note that, as mentioned earlier, loads have been normalized for numerical robustness (in this case, N_x / $N_{x,critical}$). The $N_{x,critical}$ for the plain weave carbon-epoxy in this study was found to be 6.40 x 10^3 Pa-m ; this was used to normalize all force resultant terms. The $M_{x,critical}$ used to normalize all moment resultant terms was 1.85×10^{-4} Pa-m^2. A complete table of strength values for the carbon-epoxy plain weave textile composite is shown in Table 4-1.

Remaining coefficients C_{ij} can be solved by evaluating Equation 4.4 with the maximum possible $F_i = F_j$ as determined by the DMM results. All other loads are set to zero. This reduction in terms, along with knowledge of previously determined

Table 4-1: Strength Values for Independent Load Conditions

	Strength (+)	**Strength (-)**
$\boldsymbol{N_x}$	6.40e3 Pa-m	5.86e3 Pa-m
$\boldsymbol{N_y}$	6.40e3 Pa-m	5.86e3 Pa-m
$\boldsymbol{N_{xy}}$	2.11e3 Pa-m	2.11e3 Pa-m
$\boldsymbol{M_x}$	1.85e-4 Pa-m^2	1.85e-4 Pa-m^2
$\boldsymbol{M_y}$	1.85e-4 Pa-m^2	1.85e-4 Pa-m^2
$\boldsymbol{M_{xy}}$	1.06e-4 Pa-m^2	1.06e-4 Pa-m^2

coefficients C_{ii} and $D_{i,}$ allows for the solution of all remaining coefficients. For example, C_{14} can be determined by applying the maximum possible F_1 and F_4 such that

$$F_1 = F_4 = \frac{N_x}{N_{critical}} = \frac{M_x}{M_{critical}} \tag{4.6}$$

The failure coefficient is then solved from Equation 4.4 as

$$C_{14} = \frac{1}{2F_1F_4}\left(1 - C_{11}F_1^2 - C_{44}F_4^2 - D_1F_1 - D_4F_4\right) \tag{4.7}$$

The full results of the above procedures are shown in Table 4-2 and Table 4-3 below. Note that coefficients D_3 through D_6 are equal to zero since positive and negative failure values are the same for any shear or moment loads.

For complete evaluation of the 27 failure coefficients, it will generally not be necessary to complete 27 separate physical or simulated experimental evaluations. Exploitation of geometry can lead to a significant reduction. The plain weave under investigation requires 13 evaluations to determine all coefficients, and more complicated weaves will still often exhibit symmetry such that only this amount is required. For the most general case, 27 evaluations may be required. Twelve involve a single load F_i both in tension and compression. Fifteen evaluations will be needed that involve every combination of two loads applied equally (as normalized) until failure. These 27 evaluations may be performed either by physical experiment or simulated via the DMM.

Table 4-2: Normalized Failure Coefficients C_{ij} for Quadratic Failure Equation. (Coefficient C_{mn} is in m^{th} Row and n^{th} Column)

	n = 1	**2**	**3**	**4**	**5**	**6**
m = 1	1.02	-0.81	2.45	0.15	0.15	-0.09
2		1.02	2.45	0.15	0.15	-0.09
3			9.29	0.15	0.15	-1.28
4				1.00	-0.65	0.29
5					1.00	0.29
6						3.05

Table 4-3: Normalized Failure Coefficients D_i for Quadratic Failure Equation

D_1	-0.011
D_2	-0.011
D_3	0.000
D_4	0.000
D_5	0.000
D_6	0.000

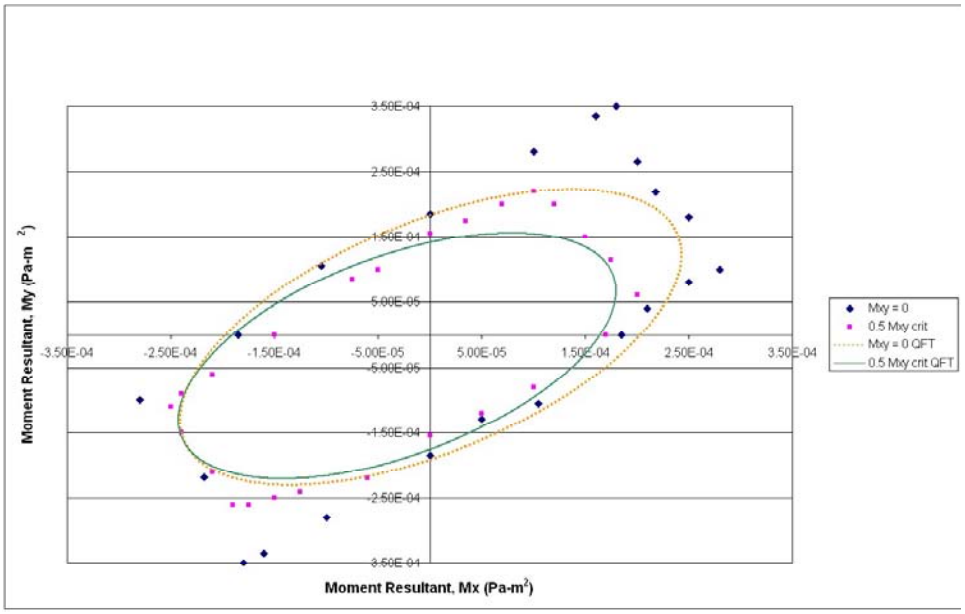

Figure 4-6: DMM Failure Envelopes for Biaxial Bending with Constant Applied Twisting Moment as Compared to the Quadratic Failure Theory Predictions.

Referring to Figures 4-6 and 4-7, the failure spaces calculated via the DMM and previously shown in Figures 3-7 and 3-8 are compared to the elliptical curves labeled

QFT, which represent the failure envelopes as predicted by the quadratic failure theory of Equation 4.4. The overall agreement in such test cases is seen to be quite suitable, but as seen in Figure 4-6, there will be "corners" or portions of the 6D failure space that will be missed with the essentially 6D ellipse space of the quadratic failure theory. In general, the QFT predictions tend to be conservative in areas of disagreement.

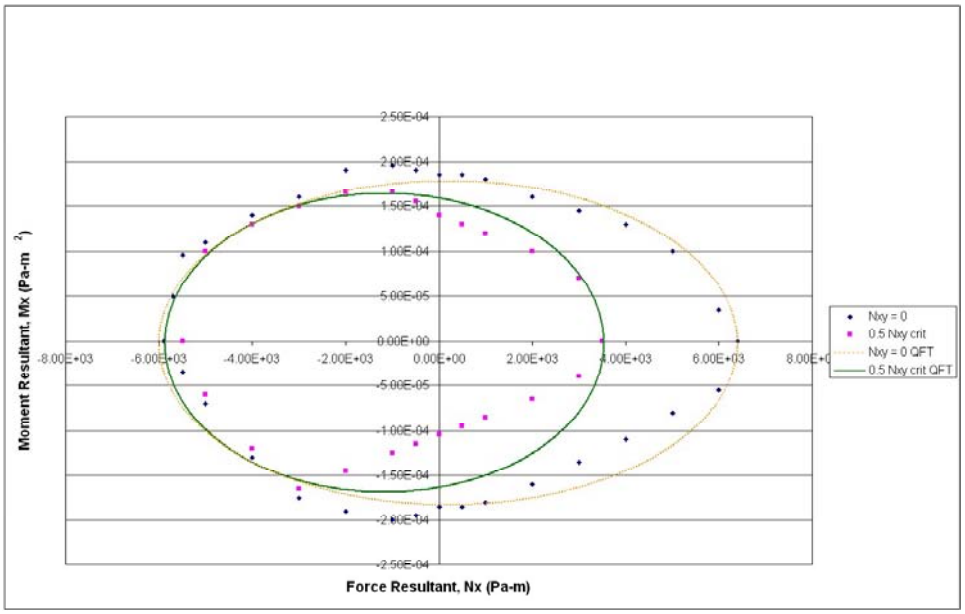

Figure 4-7: DMM Failure Envelopes with Force and Moment Resultants for Constant Applied Shear as Compared to the Quadratic Failure Theory Predictions.

For further comparison and to incorporate more complex loading conditions, several test cases were computed to determine the difference in solutions computed from Equation 4.4 as compared to the results of the DMM. In general, F_i may be populated by as many as 6 terms from among ($N_x\, N_y\, N_{xy}\, M_x\, M_y\, M_{xy}$). For cases in which 1, 2, or 3 terms are populated, the solution is accurate to within a few percent. For test cases in which 4, 5, or 6 terms are populated, the average error was seen to be 9.3%, and several example test cases are tabulated below. Care was taken to select a broad spectrum of cases such

that both positive and negative values are employed, and multiple load ratios and load types are employed. Load ratios (α) are shown to characterize the test cases, defined as

$$\alpha_i = \frac{F_i}{F_1} \tag{4.8}$$

By maintaining the same load ratios, all predicted failure loads will maintain a single ratio with respect to DMM failure points. Thus one ratio can characterize the congruence of these two solutions. A ratio of one will imply complete agreement between the two solutions. A ratio less than one indicates a conservative failure prediction, and a ratio greater than one implies the converse. Tables 4-4 through 4-6 summarize the results.

Table 4-4: Comparison of Quadratic Failure Equation Predictions with DMM Results. Test Cases Include 4 Populated Load Terms F_i

	F_1	**F_2**	**F_3**	**F_4**	**F_5**	**F_6**
α	1.00	0.00	0.92	6.67E-08	0.00	6.67E-08
DMM	1.20E+03	0.00E+00	1.10E+03	8.00E-05	0.00E+00	8.00E-05
Quadratic Theory	1.12E+03	0.00E+00	1.02E+03	7.44E-05	0.00E+00	7.44E-05
Ratio	0.93					
α	1.00	1.83	0.00	6.67E-08	0.00	6.67E-08
DMM	1.20E+03	2.20E+03	0.00E+00	8.00E-05	0.00E+00	8.00E-05
Quadratic Theory	1.24E+03	2.27E+03	0.00E+00	8.24E-05	0.00E+00	8.24E-05
Ratio	1.03					
α	1.00E+00	-0.87	0.00	3.91E-08	-1.40E-08	0.00
DMM	-2.30E+03	2.00E+03	0.00E+00	-9.00E-05	3.23E-05	0.00E+00
Quadratic Theory	-2.55E+03	2.22E+03	0.00E+00	-9.99E-05	3.59E-05	0.00E+00
Ratio	1.11					
α	1.00	0.40	0.00	1.80E-08	-6.46E-09	0.00
DMM	-5.00E+03	-2.00E+03	0.00E+00	-9.00E-05	3.23E-05	0.00E+00
Quadratic Theory	-5.50E+03	-2.20E+03	0.00E+00	-9.90E-05	3.55E-05	0.00E+00
Ratio	1.1					

α	1.00	-0.50	0.00	-1.61E-08	-8.08E-09	0.00
DMM	-4.00E+03	2.00E+03	0.00E+00	6.45E-05	3.23E-05	0.00E+00
Quadratic Theory	-3.72E+03	9.30E+02	1.53E+03	6.51E-05	6.51E-05	7.44E-05
Ratio	0.93					

Table 4-5: Comparison of Quadratic Failure Equation Predictions with DMM Results. Test Cases Include 5 Populated Load Terms F_i

	F_1	**F_2**	**F_3**	**F_4**	**F_5**	**F_6**
α	1.00	1.00	1.00	6.25E-08	0.00	6.67E-08
DMM	1.20E+03	1.20E+03	1.20E+03	7.50E-05	0.00E+00	8.00E-05
Quadratic Theory	1.04E+03	1.04E+03	1.04E+03	6.53E-05	0.00E+00	6.96E-05
Ratio	0.87					
α	1.00	1.67	1.20	4.67E-08	5.33E-08	0.00
DMM	1.50E+03	2.50E+03	1.80E+03	7.00E-05	8.00E-05	0.00E+00
Quadratic Theory	1.32E+03	2.20E+03	1.58E+03	6.16E-05	7.04E-05	0.00E+00
Ratio	0.88					
α	1.00	-1.33	-1.07	-4.67E-08	3.33E-08	0.00
DMM	-1.50E+03	2.00E+03	1.60E+03	7.00E-05	-5.00E-05	0.00E+00
Quadratic Theory	-1.32E+03	1.76E+03	1.41E+03	6.16E-05	-4.40E-05	0.00E+00
Ratio	0.88					
α	1.00	1.33	1.00	-3.33E-08	2.67E-08	0.00
DMM	-1.50E+03	-2.00E+03	-1.50E+03	5.00E-05	-4.00E-05	0.00E+00
Quadratic Theory	-1.32E+03	-1.76E+03	-1.32E+03	4.40E-05	-3.52E-05	0.00E+00
Ratio	0.88					
α	1.00	-0.45	0.45	2.27E-08	0.00	3.18E-08
DMM	-2.20E+03	1.00E+03	-1.00E+03	-5.00E-05	0.00E+00	-7.00E-05
Quadratic Theory	-2.16E+03	9.80E+02	-9.80E+02	-4.90E-05	0.00E+00	-6.86E-05
Ratio	0.98					

Table 4-6: Comparison of Quadratic Failure Equation Predictions with DMM Results. Test Cases Include 6 (Fully Populated) Load Terms F_i

	F_1	F_2	F_3	F_4	F_5	F_6
α	1.00	-1.00	1.00	4.00E-08	4.00E-08	2.00E-08
DMM	1.49E+03	-1.49E+03	1.49E+03	5.96E-05	5.96E-05	2.98E-05
Quadratic Theory	1.28E+03	-1.28E+03	1.28E+03	5.13E-05	5.13E-05	2.56E-05
Ratio	0.86					
α	1.00	1.00	0.52	1.33E-08	1.33E-08	1.33E-08
DMM	3.00E+03	3.00E+03	1.55E+03	4.00E-05	4.00E-05	4.00E-05
Quadratic Theory	2.61E+03	2.61E+03	1.35E+03	3.48E-05	3.48E-05	3.48E-05
Ratio	0.87					
α	1.00	-0.73	-0.33	-1.33E-08	1.33E-08	1.33E-08
DMM	-3.00E+03	2.20E+03	1.00E+03	4.00E-05	-4.00E-05	-4.00E-05
Quadratic Theory	-2.85E+03	2.09E+03	9.50E+02	3.80E-05	-3.80E-05	-3.80E-05
Ratio	0.95					
α	1.00	-0.67	0.67	-2.67E-08	5.33E-08	-3.33E-08
DMM	-1.50E+03	1.00E+03	-1.00E+03	4.00E-05	-8.00E-05	5.00E-05
Quadratic Theory	-1.44E+03	9.60E+02	-9.60E+02	3.84E-05	-7.68E-05	4.80E-05
Ratio	0.96					
α	1.00	0.59	0.88	3.53E-08	3.53E-08	4.71E-08
DMM	-1.70E+03	-1.00E+03	-1.50E+03	-6.00E-05	-6.00E-05	-8.00E-05
Quadratic Theory	-1.45E+03	-8.50E+02	-1.28E+03	-5.10E-05	-5.10E-05	-6.80E-05
Ratio	0.85					

Optimization of Failure Coefficients

The failure coefficients of Table 4-2 and 4-3 have been obtained from procedures designed to be compatible with physical experiments. However, further accuracy may be obtained through analytical methods to optimize the coefficients. The DMM has shown that for this particular weave pattern, a failure theory of the form of Equation 4.4 is an effective predictor of strength in multiple failure spaces, and that its inclusion of moment

resultants at the micro level represents a critical consideration. After this groundwork, the failure coefficients may be found from the above procedure either by using the DMM or physical testing, or by employing a least-squares routine which calculates the failure coefficients that maximize the accuracy of the obtained solution.

To this end, the Matlab™ subroutine "lsqnonlin" has been employed. The coefficients of Table 4-2 and 4-3 are supplied to the routine, which was then limited to its perturbation of each coefficient by a factor of ± 10%. This represents an optimization which is constrained to maintain some proximity to the physically interpretable constants of Table 4-2 and 4-3. Further perturbation could be allowed, with a danger of overfitting, but this initial study is presented to elucidate the opportunity for further optimization. As fitting data, the 15 above test cases were provided, in addition to the data from the 27 tests used to fit failure coefficients by the previous procedure, for a total of 42 fit-points. Resulting coefficients as determined by the optimization algorithm are shown in Table 4-7 and Table 4-8. Significant reduction was shown in the minimization of the error of the objective function of Equation 4.4. Over the 15 test cases of Table 4-4 through 4-6, which previously exhibited an average error of 9.3%, the optimized failure coefficients reduce error to 7.7% over these cases. Note that average error is calculated as the absolute value of deviation from a perfect prediction.

Table 4-7: Optimized Failure Coefficients C_{ij} for Quadratic Failure Equation. (Coefficient C_{mn} is in m^{th} Row and n^{th} Column)

	n = 1	**2**	**3**	**4**	**5**	**6**
m = 1	1.115	-0.891	2.205	0.135	0.135	-0.099
2		1.029	2.205	0.135	0.135	-0.099
3			8.361	0.135	0.135	-1.408
4				0.9	-0.715	0.261
5					0.9	0.261
6						2.745

Table 4-8: Optimized Failure Coefficients D_i for Quadratic Failure Equation

D_1	-0.0121
D_2	-0.099
D_3	0
D_4	0
D_5	0
D_6	0

Table 4-9: Data to Indicate Results of Coefficient Optimization

							Q-1	**Q-1**	**$(Q-1)^2$**	**$(Q-1)^2$**
index	**Normalized Force or Moment Resultants F_i**						*standard*	*optim*	*standard*	*optim*
1	0.1875	0	0.17188	0.43243	0	0.43243	0.11964	-0.0063	0.01431373	3.96887E-05
2	-0.35938	0.3125	0	-0.48649	0.17459	0	-0.03526	-0.0351	0.00124341	0.00123208
3	0.1875	0.34375	0	0.43243	0	0.43243	-0.07631	-0.01636	0.00582322	0.000267584
4	-0.78125	-0.3125	0	-0.48649	0.17459	0	-0.09002	-0.07669	0.00810414	0.005881816
5	-0.625	0.3125	0	0.34865	0.17459	0	-0.25237	-0.2142	0.06369062	0.04588164
6	0.28125	0.15625	0.25781	0.37838	0.37838	0.43243	0.73672	0.52306	0.54275636	0.273591764
7	-0.23438	0.15625	-0.15625	0.21622	-0.43243	0.27027	-0.06791	-0.01178	0.00461177	0.000138721
8	0.46875	0.46875	0.24219	0.21622	0.21622	0.21622	0.58519	0.43468	0.34244734	0.188946702
9	-0.26563	-0.15625	-0.23438	-0.32432	-0.32432	-0.43243	0.53185	0.34624	0.28286442	0.119882138
10	-0.46875	0.34375	0.15625	0.21622	-0.21622	-0.21622	-0.03722	-0.03568	0.0013854	0.001272706
11	0.1875	0.1875	0.1875	0.40541	0	0.43243	0.13935	0.096473	0.01941842	0.00930704
12	-0.23438	-0.3125	-0.23438	0.27027	-0.21622	0	0.078115	-0.01175	0.00610195	0.000138039
13	0.23438	0.39063	0.28125	0.37838	0.43243	0	0.063019	0.045837	0.00397139	0.002101031
14	-0.34375	0.15625	-0.15625	-0.27027	0	-0.37838	-0.03917	-0.01162	0.00153437	0.000135048
15	-0.23438	0.3125	0.25	0.37838	-0.27027	0	0.13059	0.064909	0.01705375	0.004213178
16	1	0	0	0	0	0	0.009	0.1029	0.000081	0.01058841
17	0	1	0	0	0	0	0.009	0.0195	0.000081	0.00038025
18	0	0	0	1	0	0	1.00E-07	-0.1	1E-14	0.01
19	0	0	0	0	1	0	1.00E-07	-0.1	1E-14	0.01
20	0	0	0.32813	0	0	0	0.000217	-0.0998	4.7228E-08	0.009960838
21	0	0	0	0	0	0.57297	0.001309	-0.09882	1.7135E-06	0.009765788
22	0	0	0	1.1892	1.1892	0	0.00913	0.05343	8.3357E-05	0.002854765
23	0.25312	0	0.25312	0	0	0	-0.01852	-0.02546	0.00034306	0.000648364
24	0	0.25312	0.25312	0	0	0	-0.01852	-0.02596	0.00034306	0.000673714
25	0	0	0	0.46486	0	0.46486	-0.00621	-0.01559	3.86E-05	0.00024311
26	0	0	0	0	0.46486	0.46486	-0.00621	-0.01559	3.86E-05	0.00024311
27	0.51	0	0	0	0	0.51	0.029588	-0.02794	0.00087545	0.000780364
28	0	0.51	0	0	0	0.51	0.029588	-0.04908	0.00087545	0.002408552
29	0.66	0	0	0.66	0	0	-0.0062	-0.07145	3.845E-05	0.005104531
30	0	0.66	0	0.66	0	0	-0.0062	-0.10728	3.845E-05	0.011508998
31	0	0	0.32	0	0	0.32	0.013254	-0.00692	0.00017567	4.79515E-05
32	0.66	0	0	0	0.66	0	-0.0062	-0.07145	3.845E-05	0.005104531
33	0	0.66	0	0	0.66	0	-0.0062	-0.10728	3.845E-05	0.011508998

34	0	0	0.66	0.66	0	0	-0.00092	0.15173	8.4839E-07	0.023021993
35	0	0	0.66	0	0.66	0	-0.00092	0.15173	8.4839E-07	0.023021993
36	1.58	1.58	0	0	0	0	9.80E-07	0.013	9.604E-13	0.000169
37	-0.91	0	0	0	0	0	8.80E-07	0.0072	7.744E-13	0.00005184
38	0	-0.91	0	0	0	0	8.80E-07	0.001404	7.744E-13	1.97122E-06
39	0	0	-0.328	0	0	0	0.000217	-0.0998	4.7228E-08	0.009960838
40	0	0	0	-1	0	0	1.00E-07	-0.1	1E-14	0.01
41	0	0	0	0	-1	0	1.00E-07	-0.1	1E-14	0.01
42	0	0	0	0	0	-0.573	0.001309	-0.09882	1.7135E-06	0.009765788
								Sum	1.31841456	0.830844875
								rms error	0.17717455	0.140648572

Table 4-9 indicates the output of the coefficient optimization routine. The first column simply indexes each of the 42 load cases used for fitting. This is followed by columns indicating the normalized force and moment resultants in each case. As before, force resultants are normalized with the critical N_x in tension, and moment resultants are normalized with respect to critical M_x. The next two columns display the evaluation of the quantity (Q-1) for each load case (where "Q" is the calculation of Equation 4.4, which should ideally produce unity at failure) as evaluated with standard or optimized failure coefficients. These columns would then display zero for a completely accurate evaluation. The final two columns display the square of this error, which is then summed and divided by 42, the square root of which then yields the indicated rms error. The optimization produces a significant improvement which, as has been mentioned, yields to an improvement in accuracy of predicted test cases.

Chapter Summary

Based upon failure envelopes constructed by analysis of the microstresses developed in a representative volume element (RVE), two alternate methods for predicting failure envelopes of a plain-weave textile composite have been developed.

The previously developed Direct Micromechanics Method (DMM) has been used to construct failure envelopes for a plain weave carbon/epoxy textile composite in plane stress. To allow for the accommodation of stress gradients, micromechanical analysis had been performed in terms of classical laminate theory force and moment resultants [*N*], [*M*] and constitutive matrices [*A*], [*B*], [*D*]. A parametric ellipse-fitting scheme which accurately predicts trends in failure envelopes for a given failure space has been developed by analysis of failure ellipse parameters. This method for predicting failure envelopes was found to agree with DMM results to within a few percent. A second method involves development of a 27-term quadratic failure criterion to predict failure under general loading conditions. The quadratic failure criterion was found to agree with DMM results within an average deviation of 9.3%, but the method is more robust in terms of its ability to predict failure from more complex loading cases.

CHAPTER 5
MULTI-LAYER ANALYSIS

The methods of the previous chapters involve characterization of the stiffness and strength of a single RVE, or a single-layer plain weave textile composite. When multiple layers are present, the layer properties will remain the same, but the stiffness and strength of the overall composite will change. To develop a fully general failure theory, these methods must be adapted to accommodate a textile composite of an arbitrary number of layers. This can be predicted through direct simulation of a layup to directly determine stiffness properties. This will yield accurate results, but creating a new FEM model for each new layup is highly impractical. Thus, the single layer characterization methods must be adapted to predict the properties of a layup of an arbitrary number of layers. This allows material characterization simulations of a single RVE to be applicable to a layup of an arbitrary number of layers, eliminating the need for further material characterization. Thus a practical tool for failure analysis and design of a plain weave textile composite has been developed.

These previous methods are adapted via three multi-layer analysis techniques: direct simulation of a multi-layer composite (which provides an accurate basis for comparison), an adjustment of the data output from single-layer FEM simulation, and implementation of the quadratic failure theory (without the requirement of determining a new set of failure coefficients). Failure points have been predicted for a variety of load cases.

The entire body of work is then applied to several practical examples of strength prediction to illustrate their implementation. The results are compared to conventional methods utilizing common failure theories not specifically developed for textile composites. Design of a dual-layer textile plate under uniform pressure is considered, for several geometries and width-to-thickness ratios. Also shown is a test case of a pressure vessel in which stress-gradients are less prevalent. Results are shown in terms of the maximum allowable pressure, as well as comparison of point-by-point factor of safety values.

Stiffness Prediction of Multi-Layer Textile Composites

A direct simulation of the behavior of a dual layer composite has been performed. The single RVE is replaced with two stacked RVE's which simulate the dual-layer textile composite. Using the procedures of Chapter 2, 6 unit strain and curvature cases have again been carried out to directly determine the mechanical response. Then macro level force and moment resultants can be computed, and the constitutive matrices are determined. Referring back to Chapter 3, a single layer of the plain weave textile under consideration will exhibit the following the following constitutive matrices

$$[A] = \begin{bmatrix} 4.14 & 0.52 & 0 \\ 0.52 & 4.14 & 0 \\ 0 & 0 & 0.18 \end{bmatrix} \times 10^{6} (Pa - m) \qquad [B] \approx 0 \qquad (5.1)$$

$$[D] = \begin{bmatrix} 7.70 & 2.53 & 0 \\ 2.53 & 7.70 & 0 \\ 0 & 0 & 1.35 \end{bmatrix} \times 10^{-3} (Pa - m^{3})$$

Now for a two-layer textile, the constitutive matrices, as determined from a two-layer model utilizing the DMM, are seen to be

$$[A] = \begin{bmatrix} 8.28 & 1.04 & 0 \\ 1.04 & 8.28 & 0 \\ 0 & 0 & 0.36 \end{bmatrix} \times 10^6 (Pa - m) \qquad [B] \approx 0 \qquad (5.2)$$

$$[D] = \begin{bmatrix} 148.8 & 22.4 & 0 \\ 22.4 & 148.8 & 0 \\ 0 & 0 & 8.51 \end{bmatrix} \times 10^{-3} (Pa - m^3)$$

The in-plane properties of the [*A*] stiffness matrix remain effectively unchanged; the doubling in value of this matrix is a bookkeeping artifact commensurate with the fact that there is twice as much material present with two layers, as compared to one. The same is true in part for the bending stiffness [*D*] as well. However, bending properties are affected by the moment of inertia of the material that is present. For the two-layer plain-weave under investigation, this represents an approximately 10-fold increase in bending stiffness per layer, or an overall 20-fold increase in bending stiffness for both layers collectively. The same amount of material present will have higher bending stiffness the further it is from the neutral axis of bending. Consequently, bending stiffness follows a relationship analogous to the Parallel Axis Theorem, which governs the increased moment of inertia of an area of material that is moved away from the bending axis. These expressions that govern the overall stiffness of a multi-layer textile can be represented as

$$A_{ij}^{DL} = 2A_{ij}^{SL} \qquad (5.3)$$

$$D_{ij}^{DL} = 2(D_{ij}^{SL} + A_{ij}^{SL} d^2) \qquad (5.4)$$

where the superscripts *DL* and *SL* represent "double layer" or "single layer" properties, and *d* represents the distance from the center of a layer to the bending axis. Similar results have been shown in [35] for textile composites under flexure. From this

expression, the double layer stiffness matrices (Equation 5.2) can effectively be calculated with knowledge only of the single layer stiffness properties (Equation 5.1). This can be extrapolated to a material of an arbitrary number of layers (N), once the DMM has been used to characterize a layer (n) or one RVE. Equation 5.5 and Equation 5.6 may be used to evaluate the stiffness matrices and no further analysis is needed.

$$A_{ij} = \sum_{n=1}^{N} A_{ij}^{n} \tag{5.5}$$

$$D_{ij} = \sum_{n=1}^{N} (D_{ij}^{n} + A_{ij}^{n} d_{n}^{2}) \tag{5.6}$$

Strength Prediction of Multi-Layer Textile Composites

Once stiffness has been determined by the methods of the previous section, strength of a multi-layer textile may be determined. The following three sub-sections describe the various modeling approaches used to analyze laminated plain weave composite structures and comparison of various methodologies in modeling the strength of textile composites. For clarity, the various approaches are summarized in Table 5-1.

Table 5-1: Summary of the Various Methods Employed in Multi-Layer Strength Analysis

Method	**Acronym**	**Summary**
Direct Micromechanics Method	DMM	Method of chapter 2, used to characterize strength and stiffness of an RVE
Dual Layer Direct Micromechanics Method	DDMM	Direct simulation of two stacked RVE's, used to characterize multiple layers
Adapted Direct Micromechanics Method for Dual Layer Analysis	ADMM	Method to adapt data output from the DMM to obtain multiple layer strength prediction
Quadratic Failure Theory	QFT	Method for implementing the quadratic failure theory introduced in chapter 4

Direct FEM Simulation of Multi-Layer Textile Composites Using the DMM for Failure Analysis ("DDMM")

The same methods described above for single layer strength prediction can be used for direct simulation of a two layer RVE. This direct simulation paints an accurate picture of the load capacity of a multilayer textile, at the expense of model preparation and calculation time. As the methods for the DDMM approach are essentially the same as the DMM described in Chapter 2, with a dual-layer RVE in place of the single RVE, the details are not repeated. The two sections to follow then describe two methods based upon these results (ADMM and QFT) which can be used to predict strength of a textile composite of an arbitrary number of layers without having to employ direct FEM simulation.

Through the DDMM, it is seen that, as also seen for stiffness properties, the in-plane strength properties do not change. The critical force resultant doubles as a result of the doubling of material present, but otherwise the load capacity is unchanged.

$$N_{ij,crit}^{DL} = 2N_{ij,crit}^{SL} \tag{5.7}$$

Here the subscript *crit* denotes the critical load that is the maximum allowable when all other loads are zero (or the strength for each individual load type N_{ij}). As previously seen, the superscripts *DL* and *SL* represent associations with single-layer or dual-layer properties, respectively.

The strength under bending will change significantly for the two-layer textile. As a direct consequence of increased bending stiffness, the critical applied moment is seen to increase tenfold.

$$M_{ij,crit}^{DL} \approx 10M_{ij,crit}^{SL} \tag{5.8}$$

Note that this relationship will depend on the thickness of each layer, and thus is an observation specific to this RVE micro geometry (conversely, Equation 5.7 will be true for comparing single and double layer properties for any thickness).

The DDMM serves as a check upon which a more generalized approach may be developed, which can predict for an arbitrary number of layers under arbitrary load conditions with mixed load types (not simply mono-loading cases of one critical force or moment resultant).

Adaptation of the Single Layer DMM Results to Predict Strength for Multi-Layer Textile Composites ("ADMM")

This method for taking the results of single layer material characterization and analysis and using them for multi-layer strength prediction involves adapting the results of single layer FEM analysis directly from the DMM. Thus only one material characterization is needed (single layer) to predict strength for any number of layers.

In general, using the DMM, the stress field from an applied load is calculated by determining the resultant strains and curvatures, then superposing scaled multiples of the single-layer stress field resulting from each unit strain or curvature. In the case of a single layer under bending, the sole "stress source" is the resulting curvature, thus the resulting stress field can be calculated by scaling the stress field from a single layer under unit curvature. Now in the case of two layers under bending, this stress source of curvature is still present, but there is an additional stress source that must be accounted for. Normal strains will result from the layer offset from the axis of bending. Thus scaled multiples of these unit strain cases must also be applied to find the total stress field for a multi-layer textile under bending.

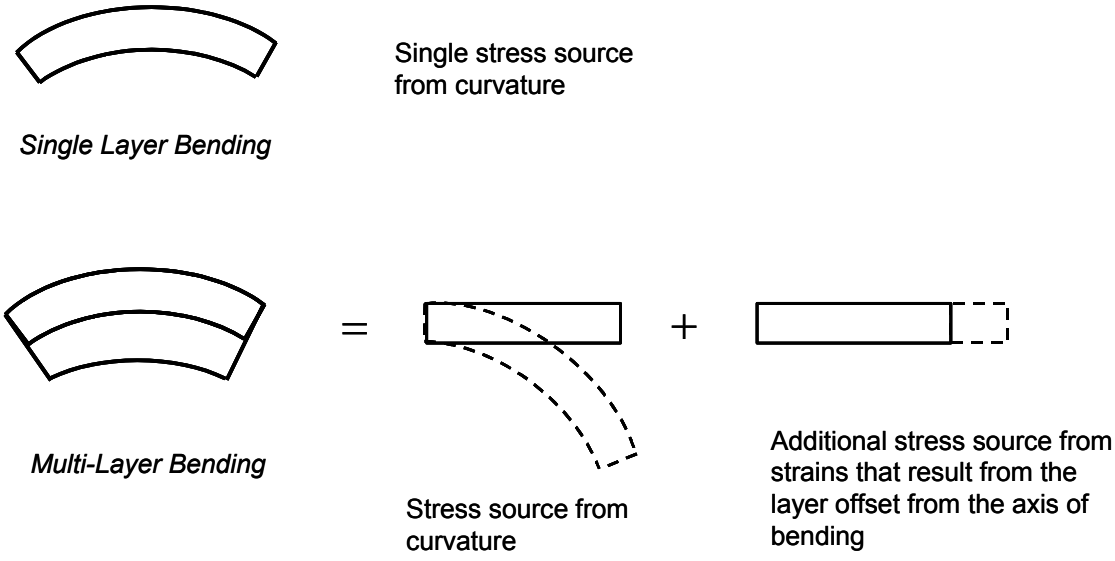

Figure 5-1: Schematic Illustration of the Single-Layer Strain and Curvature Stress Fields (As Found via the DMM) That Must Be Superposed in Calculation of the Total Stresses Resulting from Multi-Layer Bending

As detailed in classical laminate theory [34], the magnitude of the normal strain in offset layers will be directly proportional to the curvature (κ) that is present and the distance from the layer midplane to the bending axis (d).

$$\varepsilon_{ij} = \pm d\kappa_{ij} \tag{5.9}$$

This strain will be tensile or compressive (positive or negative) depending on the position of the layer with respect to the bending axis.

The failure envelope for any force and moment resultants can be determined using the above procedure. To briefly illustrate the procedure, consider a two-layer textile under bending, with an x-curvature of 0.5 and a layer thickness of 0.2. Then the total stress field is found by superposing scaled multiples of the stress fields resulting from unit strain ($\sigma_{ij}^{\varepsilon=1}$) and curvature ($\sigma_{ij}^{\kappa=1}$) cases

$$\begin{aligned} \sigma_{ij} &= \kappa_x \sigma_{ij}^{\kappa_x=1} \pm d\kappa_x \sigma_{ij}^{\varepsilon_x=1} \\ \sigma_{ij} &= 0.5\sigma_{ij}^{\kappa_x=1} \pm \left(\tfrac{0.2}{2}\right)(0.5)\sigma_{ij}^{\varepsilon_x=1} \end{aligned} \tag{5.10}$$

where the "±" indicates that the stress field in the tensile layer will be calculated as the sum of the two terms in each equation, and conversely, stress in the compressive layer will be calculated as the difference of the two stress fields.

As detailed earlier, failure from the total stress field in each layer is then checked on an element-by-element basis to determine overall failure of the composite. Proveout and comparisons of this method will be shown after the next section.

Implementation of the Quadratic Failure Theory to Predict Strength for Multi-Layer Textile Composites ("QFT")

The previously developed 27-term quadratic failure theory for textile composites, as determined from the single-layer DMM, can be implemented to predict failure for a multi-layer specimen. Once the original failure coefficients have been determined, no further FEM or experimental analysis will be needed. Implementation of this procedure is accomplished by adjusting the force and moment resultants applied to the multi-layer specimen to reflect the true stress state in each layer, on a layer-by-layer basis. First, the mid-plane multi-layer strain and curvature are calculated from the applied macro-level force and moment resultant, along with the constitutive matrix representing the double-layer (*DL*) material properties.

$$\begin{Bmatrix} [\varepsilon_o] \\ [\kappa] \end{Bmatrix} = \begin{bmatrix} [A] & [B] \\ [B] & [D] \end{bmatrix}_{DL}^{-1} \begin{Bmatrix} [N] \\ [M] \end{Bmatrix} \tag{5.11}$$

The dual-layer midplane strain must now be modified to represent the actual strain state in each layer.

$$\varepsilon_{ij} = \varepsilon_o \pm d\kappa_{ij} \tag{5.12}$$

Note that in plate analysis, mid-plane curvature and layer-level curvature will always be the same, as curvature is always constant through-thickness for a given layup, regardless of thickness or number of layers (although strains may show variation).

The layer-level force and moment resultant are then calculated using this modified strain from Equation 5.12, along with the single layer (*SL*) constitutive matrix.

$$\begin{Bmatrix}[N]\\[M]\end{Bmatrix}_{SL} = \begin{bmatrix}[A] & [B]\\[B] & [D]\end{bmatrix}_{SL} \begin{Bmatrix}[\varepsilon]\\[\kappa]\end{Bmatrix} \tag{5.13}$$

The adjusted force and moment resultants capture what is seen in each layer offset from the bending axis. These are then directly input to the quadratic failure theory of Equation 4.4 with coefficients as per Table 4-2 and 4-3 (as developed from one layer or RVE). Failure analyses are performed independently in each layer. This is to say that, the single layer force and moment resultants for each layer must be independently calculated input to the quadratic failure theory (computations which can still be automated). Note that, via the above procedure, a pure moment resultant applied to the two-layer composite will correspond to both a force and moment resultant in each layer.

Comparison of the Results of Multi-Layer Failure Analysis Methods

Several cases are now presented which illustrate the relative effectiveness of the multi-layer analysis methods shown in the preceding sections of this chapter. Direct FEM simulation provides the most accurate prediction of the stress field and failure envelope of the multi-layer textile. Thus the two techniques for predicting failure of a multi-layer composite without additional material characterization tests can be compared to this in order to estimate their accuracy.

One method of comparison is to look directly at the predicted stress field under several loading conditions. However, these point-by-point (or element-by-element)

comparisons prove to be not the most effective summarization of accuracy. Comparison of a few points can yield an inaccurate sample of results that appear to differ greatly, even if the majority of the stress field compares quite closely. However, comparison of the calculated stresses at many (or all) points and taking an average accuracy is not necessarily the best metric either, as standard deviation could potentially be large. Thus, certain portions of the stress field might be predicted very well, whereas certain portions might not be accurately predicted. In this case, an average of point-by-point stress deviation might appear small, but in fact such situation should not be considered as an accurate prediction. Furthermore, some predicted stress components at a given point might compare well to direct simulation, whereas other components do not, which opens the door for further ambiguity. This having been said, in general, in a point-by-point comparison, it has been observed that predicted stress fields generally show an average accuracy on the order of 90% with roughly 10% standard deviation for the two prediction methods (ADMM and QFT) as compared to direct simulation (DDMM).

Comparison of predicted failure points (the maximum allowable force and moment resultants under combined loading) proves to be the best and most germane method of comparing the multiple prediction methods. To this end, failure has been predicted for a variety of load cases based on the data from the direct simulation of the DDMM. The results of the ADMM and the QFT are then compared to this. Both methods are shown to compare well to the DDMM results, though use of the QFT is computationally faster and more practical once failure coefficients have been determined. Table 5-2 and Table 5-3 below show a comparison of the various methods to calculate failure for a multi-layer textile. As in Chapter 4, load cases are shown in terms of a Load Ratio (α) defined as

$$\alpha_i = \frac{F_i}{F_1} \tag{5.14}$$

As introduced in Chapter 4, by maintaining the same load ratios, all predicted failure loads will maintain a single ratio with respect to DDMM failure points. Thus one ratio can characterize the congruence of these solutions. A ratio of one will imply complete agreement. A ratio less than one indicates a conservative failure prediction, and a ratio greater than one implies a non-conservative prediction.

The last two failure prediction comparisons of Table 5-3 are shown in different terms in order to employ a more effective normalization which accommodates the incongruity of the magnitude of force resultants and moment resultants. In these two cases, failure points are found for which

$$\frac{N_{i,crit}}{A} = \frac{M_{i,crit}}{A} \tag{5.15}$$

for an unknown value A at failure. The first case, indicated by a (+) in Table 5-2, is the solution for failure in the tensile layer, in which the applied moment generates tensile forces that accelerate failure. The second case, indicated by a (-) , is the solution for failure in the compressive layer, in which case the applied moment offsets applied tensile force resultants. This approach also essentially solves for the factor by which load capacity changes when the additional load is applied. In other words, an A of 0.48 in the compressive layer implies that twice as much force resultant may be applied to the compressive layer before failure, when compared to the failure load under no applied moment. Conversely, in the tensile layer, the A of 2.01 indicates that the additional load M_x accelerates failure such that the allowable N_x is halved (this becomes the limiting case for ultimate failure).

Table 5-2: Example Load Cases to Determine the Accuracy of Multi-Layer Analysis Methods. Accuracy is Indicated by a Ratio as Compared to DDMM Results.

	DDMM	**ADMM**	***Accuracy***	**QFT**	***Accuracy***
α					
1	1.35E+04	1.31E+04	0.97	1.30E+04	0.96
0	0	0		0	
0	0	0		0	
0	0	0		0	
0	0	0		0	
0	0	0		0	
1	1.91E+04	2.01E+04	1.05	2.02E+04	1.06
1	1.91E+04	2.01E+04		2.02E+04	
0	0	0		0	
0	0	0		0	
0	0	0		0	
0	0	0		0	
0	0	0		0	
0	0	0		0	
1	4.23E+03	4.14E+03	0.98	4.18E+03	0.99
0	0	0		0	
0	0	0		0	
0	0	0		0	
1	3.73E+03	3.52E+03	0.94	3.42E+03	0.92
1	3.73E+03	3.52E+03		3.42E+03	
1	3.73E+03	3.52E+03		3.42E+03	
0	0	0		0	
0	0	0		0	
0	0	0		0	

The Adjusted DMM and the Adjusted QFT show 5.2% and 5.5% error, respectively over these load cases. Most often, this error is conservative in comparison to the direct FEM simulation.

Table 5-3: Further Example Load Cases (Including Moment Resultants) to Determine the Accuracy of Multi-Layer Analysis Methods. Accuracy is Indicated by a Ratio as Compared to DDMM Results.

	DDMM	**ADMM**	***Accuracy***	**QFT**	***Accuracy***
α					
0					
0					
0					
1	1.68E-03	1.60E-03	0.95	1.54E-03	0.92
0					
0					
0					
0					
0					
1	2.59E-03	2.67E-03	1.03	2.72E-03	1.05
1	2.59E-03	2.67E-03		2.72E-03	
0					
N/A (+)	2.01	2.08	1.03	1.9	0.95
0					
0					
M/A	2.01	2.08		1.9	0.95
0					
0					
N/A (-)	0.48	0.44	0.92	0.42	0.88
0					
0					
M/A	0.48	0.44		0.42	0.88
0					
0					

Practical Examples to Illustrate Strength Prediction of a Two-Layer Textile Composite Plate

In order to show the application of the preceding failure prediction approaches to practical examples, design of a two-layer plain weave-textile plate is considered. Also shown is an example of a closed-end thin-walled pressure vessel. Classical analysis

procedures are employed to determine the loads that are then input to the various failure analysis techniques.

As shown in Figure 5-2, a uniform pressure is applied to a simply-supported plate. Three different plate sizes, as shown in Table 5-4, are considered to explore the different mechanical regimes of varying width-to-thickness ratios and to consider a square versus rectangular geometry. Plate Theory [36] is employed to determine the loads at each point in the plate, which are then checked for failure.

Once moments and curvatures (per unit pressure) have been determined from SDPT, failure in the plate is analyzed via several methods. From this, the maximum allowable pressure can be determined, and results for each method are compared. The most reliable method is direct simulation through the DDMM. This again provides a basis of comparison for the remaining methods.

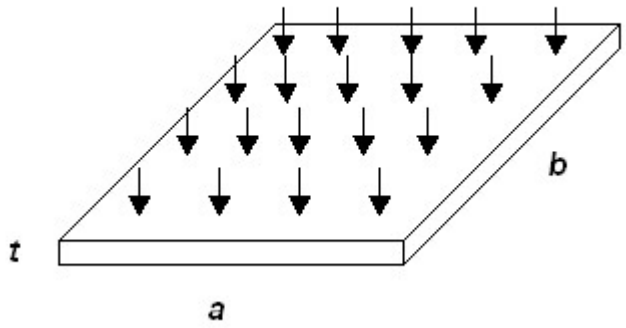

Figure 5-2: Schematic of the Simply Supported Textile Plate under Uniform Pressure

Table 5-4: Geometry of the Simply Supported Textile Plate under Uniform Pressure

	a	***b***	***t***
Case 1	0.102 m	0.102 m	0.508 mm
Case 2	0.0102 m	0.0102 m	0.508 mm
Case 3	0.102 m	0.051 m	0.508 mm

The second method represents a conventional approach, which employs failure analysis methods not developed for textile composites, and for which stress gradients are not considered. Classical analysis techniques are used to find strains and stresses, which are compared to a conventional failure theory. The third method is the Quadratic Failure Theory developed in Chapter 4. The fourth method is the aforementioned ADMM. For each case, the plate is discretized into a 21 by 21 point grid of points that are each checked for failure (441 total points).

The conventional method is accomplished by determining the curvature per unit pressure at each point via the SDPT. Strain is then determined by Equation 5.12 as per classical laminated plate theory. Stress is calculated by approximating a stiffness matrix [Q] from the [A] matrix, that was determined via the DMM as indicated by Equation 5.16, and multiplying by the corresponding strain. It should be noted that this in itself an represent an improvement over conventional methods, as a stiffness matrix would generally be calculated from homogenized material properties or estimations rather than from direct simulation or experiment. (However, unlike bending properties, these methods can often be acceptable for in-plane stiffness properties).

$$\sigma = Q\varepsilon \approx At\varepsilon \tag{5.16}$$

in which t is the thickness of a layer and A represents the in-plane stiffness matrix of a layer. This stress can then be compared to a maximum allowable stress via the Tsai-Wu Failure Theory (for which failure coefficients can be found via the DMM or experimental methods).

The procedures for the direct simulation (DDMM) as well as the QFT and ADMM methods have been detailed above, which is not repeated. In these cases, the maximum

allowable moment per unit pressure is found, and the maximum allowable pressure can then be compared. Note that in the direct two-layer DDMM, the stress field in both layers is treated as a whole, thus failure is not calculated per layer.

Tables 5-5 through 5-7 below tabulate the maximum allowable pressure for each of the three geometries under consideration, for each of the four prediction methods. The critical pressure for the compressive as well as tensile side (limiting case) of the plate in bending are shown. The relative accuracy of prediction is indicated as a ratio with respect to the DDMM direct simulation. A ratio greater than one indicates a non-conservative prediction.

Table 5-5: Maximum Pressure for the Textile Plate of Figure 5-2 with the Case 1 Geometry of Table 5-14 as Predicted from Various Multi-Layer Analysis Methods

	Case 1 (a = b , a/t = 200)		
	p_{max} **(+) (kPa)**	p_{max} **(-) (kPa)**	***Ratio/DDMM***
DDMM	19.5	n/a	-
Conventional	24.0	27.0	1.23
QFT	20.5	22.7	1.05
ADMM	20.1	22.3	1.03

Table 5-6: Maximum Pressure for the Textile Plate of Figure 5-2 with the Case 2 Geometry of Table 5-14 as Predicted from Various Multi-Layer Analysis Methods

	Case 2 (a = b , a/t = 20)		
	p_{max} **(+) (kPa)**	p_{max} **(-) (kPa)**	***Ratio/DDMM***
DDMM	135.3	n/a	-
Conventional	169.1	189.2	1.25
QFT	142.1	154.8	1.05
ADMM	139.4	153.5	1.03

Table 5-7: Maximum Pressure for the Textile Plate of Figure 5-2 with the Case 2 Geometry of Table 5-14 as Predicted from Various Multi-Layer Analysis Methods

	Case 3 (a/b = 2, a/t = 200)		
	p_{max} (+) (kPa)	p_{max} (-) (kPa)	***Ratio/DDMM***
DDMM	34.7	n/a	-
Conventional	40.6	45.5	1.17
QFT	32.6	36.2	0.94
ADMM	33.7	37.1	0.97

For all three cases, the QFT and ADMM represent a significant improvement over the conventional approach. This is due to the presence of significant stress gradients across the thickness dimension of the RVE (as accounted for with the moment resultant matrix), contrary to common isostrain assumptions used in textile micromechanics or failure theory development. The relative accuracy of conventional methods increases somewhat for Case 3. The disparity between the conventional and DMM-based approaches, which include consideration of stress gradients, will diminish as the relative presence of stress gradients diminish with respect to other loads present.

In general, the ADMM will be more accurate than the QFT, as the QFT is an approximation method which is slightly further removed from the developmental data. Though both methods involve multi-layer approximations, the QFT must also approximate the DMM stress field data. For Case 1 versus Case 2, the agreement of the two mutli-layer analysis methods (ADMM or QFT) with the direct FEM simulation is similar, for both mechanical regimes. Although the low aspect ratio plate is naturally able to withstand a much higher pressure, prediction accuracies are similar. These predictions are both non-conservative, though Tables 5-2 and 5-3 have shown that this is not generally true. For Case 3, these methods are conservative compared to the DDMM.

In this case, at the failure point, there is a different load ratio ($M_x = 2M_y$, rather than the $M_x = M_y$ of Case 1 and 2), thus a different portion of the failure space is being predicted.

As most often seen in the results of Chapter 3, the initial failure mode for these design cases is transverse failure of the fiber tow, beginning in the tensile layer. This represents a fiber pull-apart initiation, or an intra-tow matrix cracking. For the unbiased ($M_x = M_y$) biaxial bending of Cases 1 and 2, failure initiates in both fiber tows, as the transverse stresses will be equal for both tows.

Tables 5-8 through 5-11 below further elucidate the failure initiation of the design cases by illustrating the Factor of Safety (ratio of allowable pressure with respect to the failure point) at several points on the plate. Only one quarter-section of the plates is considered, due to the symmetry of the plates and of the resulting stress field. The bottom-rightmost cell represents the plate center. Position is defined as a fraction of the total width dimension, such that a position of (0.5,0.5) represents the center of the plate. Although the maximum allowable pressure will differ, the difference in the distribution of factor of safety in Case 1 and 2 will be negligible and is thus co-tabulated.

Case by case, both the QFT and conventional methods yield a similar distribution of factor of safety, although the QFT shows a greater variation in the center-to-edge

Table 5-8: Case 1 and 2 Factor of Safety Across the Plate as Determined via the Conventional Approach

Position	**0**	**0.09**	**0.18**	**0.27**	**0.36**	**0.43**	**0.5**
0	∞	∞	∞	∞	∞	∞	∞
0.09	∞	4.81	3.03	2.50	2.28	2.20	2.24
0.18	∞	3.03	2.31	1.86	1.68	1.30	1.62
0.27	∞	2.50	1.86	1.58	1.40	1.33	1.32
0.36	∞	2.28	1.68	1.40	1.25	1.18	1.16
0.43	∞	2.20	1.60	1.33	1.18	1.10	1.07
0.5	∞	2.24	1.62	1.32	1.16	1.07	1.00

Table 5-9: Case 1 and 2 Factor of Safety Across the Plate as Determined via the QFT

Position	0	0.09	0.18	0.27	0.36	0.43	0.5
0	∞	∞	∞	∞	∞	∞	∞
0.09	∞	7.99	4.81	3.81	3.36	3.04	3.07
0.18	∞	4.81	3.03	2.31	1.99	1.71	1.75
0.27	∞	3.81	2.31	1.86	1.58	1.35	1.33
0.36	∞	3.36	1.99	1.58	1.40	1.18	1.14
0.43	∞	3.04	1.71	1.35	1.18	1.10	1.06
0.5	∞	3.07	1.75	1.33	1.14	1.06	1.00

Table 5-10: Case 3 Factor of Safety Across the Plate as Determined via the Conventional Approach

Position	0	0.09	0.18	0.27	0.36	0.43	0.5
0	∞	∞	∞	∞	∞	∞	∞
0.09	∞	6.74	4.04	3.16	2.77	2.48	2.49
0.18	∞	4.80	2.72	2.05	1.75	1.51	1.49
0.27	∞	4.12	2.30	1.71	1.44	1.21	1.17
0.36	∞	3.94	2.17	1.59	1.33	1.10	1.05
0.43	∞	3.88	2.13	1.56	1.29	1.06	1.00
0.5	∞	3.99	2.18	1.58	1.30	1.06	1.00

Table 5-11: Case 3 Factor of Safety Across the Plate as Determined via the QFT

Position	0	0.09	0.18	0.27	0.36	0.43	0.5
0	∞	∞	∞	∞	∞	∞	∞
0.09	∞	6.90	4.15	3.25	2.85	2.55	2.57
0.18	∞	4.86	2.77	2.09	1.79	1.55	1.53
0.27	∞	4.14	2.32	1.73	1.46	1.24	1.20
0.36	∞	3.92	2.17	1.60	1.34	1.12	1.07
0.43	∞	3.83	2.11	1.55	1.29	1.06	1.01
0.5	∞	3.90	2.14	1.56	1.29	1.06	1.00

magnitude of factor of safety. Note that factor of safety rises to infinity in the topmost row and leftmost column which represent the simply-supported edge of the plate, as the bending moment and curvature are theoretically zero here. Also note that the maximum pressure to which each factor of safety is normalized will be different for the different prediction methods. Along any "radial" path from center to edge of the plates, factor of safety is seen to be nearly inversely proportional to grid position. This trend remains for all calculation methods, over all geometry cases.

In contrast to the design of a textile plate under uniform pressure, there are other common design cases for which there would be no improvement in accuracy in employing the QFT or ADMM rather than conventional methods. For example, in designing a thin-walled pressure vessel (see Figure 5-3 and Table 5-12), a biaxial stress state with negligible stress gradients will exist. In this case, conventional methods will predict similar maximum allowable pressure when compared to the QFT or ADMM.

Stresses and stress distributions are found from basic pressure vessel theory [37]. Force resultants and moment resultants (which result from a slight radial stress distribution and will be quite small) can then be easily calculated from this result. Note that since there is no curvature, the multi-layer analysis ADMM and adjustments to the QFT inputs (as detailed in previous sections) will not be needed. Thus, this example serves as a comparison of the DDMM simulation and the QFT, contrasted to conventional methods, for a test case in which stress gradients are small. Results for this design case are shown in Table 5-13 below.

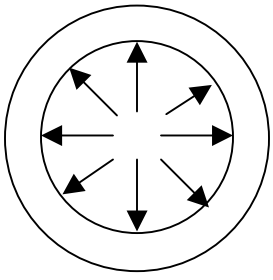

Figure 5-3: Schematic of the Dual-Layer Textile Pressure Vessel

Table 5-12: Geometry of the Textile Pressure Vessel

	radius (r)	***thickness (t)***
Case 4	10.2 mm	0.508 mm

Table 5-13: Maximum Pressure for the Textile Pressure Vessel of Figure 5-3 with the Geometry of Table 5-12 as Predicted from Various Multi-Layer Analysis Methods

	Case 4 (r/t = 20)	
	p_{max} **(MPa)**	***Ratio/DDMM***
DDMM	1.89	-
Conventional	1.93	1.02
QFT	1.86	0.98

As expected, it is seen that predicted maximum allowable pressures are similar for all methods. Although there are stress gradients along the radial direction, the variation is relatively small, thus the moment resultant that is present will be nearly negligible. These results will hold true for any thin-walled pressure vessel.

Chapter Summary

For analysis of textile composites of an arbitrary number of layers, the methods of previous chapters have been adapted. Through the results direct FEM simulation, stiffness of a multi-layer textile has been shown to be governed through an expression similar in form to that of the Parallel Axis Theorem. For the plain-weave textile under investigation, this represents a roughly 20-fold increase in stiffness when thickness is increased from one to two layers. For strength prediction, two analysis methods have been presented, again based upon and presented in comparison to the results of direct FEM simulation. The adapted single layer Direct Micromechanics Method (ADMM) is based upon a correction to the stress field as determined by the DMM (see Chapter 3) commensurate with the layer-by-layer strains which result from the offset from the axis of bending. A method for employing the quadratic failure theory (QFT, see Chapter 4) has also been developed. Without the need to modify the single-layer failure coefficients,

the inputs to the QFT are adapted to represent the true strain and curvature in each layer that is offset from the bending axis. Both the ADMM and QFT methods have been shown to predict multi-layer failure within roughly 5% accuracy.

Several simple but significant design cases have been presented as a practical application of the methods presented in this dissertation. Multi-layer failure prediction methods have been shown to be sufficiently accurate, and the importance of the consideration of stress gradients in a common design situation is shown.

CHAPTER 6
CONCLUSIONS AND FUTURE WORK

In this paper, robust methods have been developed for predicting stiffness and strength of multi-layer textile composites, with techniques designed to address the difficulties that arise when considering a textile microstructure. Currently existing failure criteria for composite materials are generally developed for and based upon usage with unidirectional composite laminates. Though these theories may to some extent be applied in an adapted form to the analysis of textile composites, as has been shown herein, many inherent simplifying assumptions no longer apply. Given the increased complexity of analysis of textile composites, there are several outstanding issues with regards to textile composites that have been addressed in this research. One of the most important issues addressed here is a robust model for prediction of strength. Though much attention has been given to the prediction of stiffness, little work has focused upon strength prediction for textile composites.

Additionally, conventional micromechanical models for textile composites assume that the state of stress is uniform over a distance comparable to the dimensions of the representative volume element (RVE). However, due to complexity of the weave geometry, the size of the RVE in textile composites can be large compared to structural dimensions. In such cases, severe non-uniformities in the stress state will exist, which conventional models do not account for. Methods for including the consideration of stress gradients have been developed, and the importance of such considerations has been demonstrated.

Stiffness properties have been predicted for a plain-weave textile composite. The results indicate good agreement with expected values from literature and material supplier data. The constitutive matrices have been calculated directly from the micromechanics model without any assumptions as in traditional plate theories. The results are quite different from commonly employed approximations. By comparison to the direct micromechanics results of the DMM, conventional methods will misrepresent flexural stiffness values D_{11}, D_{12}, and D_{66} by as much as factors of 2.9, 1.1, and 0.7 respectively. The DMM results imply that there is no consistent relation between in-plane and flexural properties, although the two properties are related.

Failure envelopes have been presented and the comparisons to and improvements over conventional methods have been shown. Under relatively simple loading conditions in which no stress gradients are present across the RVE, the DMM failure envelope was shown to compare most closely with the Tsai-Wu Failure Theory. The Maximum Stress Failure Theory and Maximum Strain Failure Theory were less close in comparison. Fiber pull-apart or failure of the transverse fiber tows was shown to be the dominant mode of failure. In limited instances of large biaxial stresses, failure of the interstitial matrix was seen to be the mode of initial failure.

Further failure envelopes have been presented which illustrate the importance of consideration of stress gradients, and the inability of conventional failure models to account for this load type. In these cases, traditional failure prediction methods can greatly overpredict the failure envelope. The presence of applied moment resultants [M], as would exist in cases of non-uniform load across the RVE, was shown to have a

significant effect on the failure envelope. Thus its consideration, not covered in conventional failure models, can be critical.

Based upon failure envelopes constructed by analysis of the microstresses developed in a representative volume element (RVE), alternate methods for predicting failure envelopes of a plain-weave textile composite have been developed. A parametric ellipse-fitting scheme which accurately predicts trends in failure envelopes for a given failure space has been developed by analysis of failure ellipse parameters. This method for predicting failure envelopes was found to agree with DMM results to within a few percent. However, it is impractical in its implementation, and is limited to consideration of one particular failure space in which only three concurrent force or moment resultants may be considered at once. The method is useful for a solid visualization and lends itself to a firm understanding of simpler load cases. A second method involves development of a 27-term quadratic failure criterion to predict failure under general loading conditions. The quadratic failure criterion was found to agree with DMM results within an average deviation of 9.3%, but the method is more robust in terms of its ability to predict failure from more complex loading cases.

The methods thusfar have been further modified to accommodate analysis of textile composites of an arbitrary number of layers. Stiffness of a multi-layer textile has been shown to be governed through an expression similar in form to that of the Parallel Axis Theorem. For strength prediction, two analysis methods have been presented. The adapted single layer Direct Micromechanics Method (ADMM) is based upon a correction to the stress field as determined by the DMM. A method for employing the quadratic failure theory (QFT) has also been developed. Both the ADMM and QFT methods have

been shown to predict multi-layer failure within roughly 5% accuracy. This adaptation thus allows for methods for the accurate prediction of strength of a multi-layer textile with a minimum of characterization requirements based upon micromechanics of a single RVE.

Finally, several design cases have been presented as a practical application of the methods presented in this dissertation. Multi-layer failure prediction methods have been shown to be sufficiently accurate, and the importance of the consideration of stress gradients in a common design situation is shown. For a simple design case of a two layer textile pressure vessel, a state of biaxial force resultant with negligible stress gradients exists. In this case, the OFT and conventional methods predict a similar allowable pressure. In consideration of the design of several textile plates of varying geometries under uniform pressure, significant stress gradients exist. Conventional methods will overpredict allowable pressures by 17% to 25%, whereas the DMM based QFT method will predict strength within 5% to 6% accuracy.

Several suggestions are offered here for potential future work that may be completed to extend the current body of work, both in terms of further development and in terms of useful application.

Incorporating a model of progressive failure represents one potential issue for future consideration. After initial failure, a component may still retain some stiffness and load bearing capacity. Continued loading leads to a progressive property loss as more and more of the constituent material becomes degraded. This can be simulated within the finite element micromechanical model by redefinition of the stiffness matrix (or

redefinition of material properties) after single element failures. The simulation is then rerun, and additional element stiffness matrices are appropriately recalculated as additional element failures occur.

Incorporation of thermal stresses and investigation of the coefficient of thermal expansion is another potential avenue for further development of the failure modeling. Due to mismatches between the coefficient of thermal expansion of constituent materials, thermal stresses can build up during manufacture or during operation. This makes inclusion of such effects critical to the accuracy of a strength prediction model. Furthermore, textile composites have been shown to perform well compared to other composites at cryogenic temperatures. Thus investigation of such thermal effects should be of considerable interest.

In the current work, the plain-weave architecture has been used to develop and demonstrate an effective micromechanical methodology and failure theory for textile composites. The same methods can easily be used to investigate the mechanical behavior of other textile weave or braid patterns. In these cases, the RVE will be larger and more complicated, but the DMM approach remains the same. Further, given that other architectures are geometrically larger, it stands to reason that the importance of stress gradient effects as presented herein will be of even greater importance.

The DMM could also be employed to perform a parametric study of the effect of weave architecture and geometry on mechanical behavior. For example, successive characterizations of the same weave type with varying two spacing, or tow undulation, etc. could provide a useful insight into the effect these parameters have on the stiffness

and strength properties of a textile composite. This could also potentially lead to the ability to optimize the microarchitecture to a specific application.

APPENDIX
PERIODIC BOUNDARY CONDITIONS

The derivation of periodic boundary conditions for unit extension and unit shear is presented here. Unit curvature has been presented in the text in Chapter 2.

Unit Extension

From the definition of strain, and utilizing integration

$$\varepsilon_x = \frac{\partial u}{\partial x} = 1$$
$$u(x, y, z) = x + c$$

$$u(a, y, z) = a + c$$
$$u(0, y, z) = c$$

$$u(a, y, z) - u(0, y, z) = a$$

Unit Shear

$$\gamma_{xy} = \frac{\partial u}{\partial y} + \frac{\partial v}{\partial x} = 1$$
$$\text{Assuming } \frac{\partial u}{\partial y} = \frac{\partial v}{\partial x},\ \frac{\partial u}{\partial y} = \tfrac{1}{2}$$
$$u(x, y, z) = \tfrac{1}{2} y + c$$

$$u(x, b, z) = \tfrac{1}{2} b + c$$
$$u(x, 0, z) = c$$

$$u(x, b, z) - u(x, 0, z) = \tfrac{1}{2} b$$

Similarly,

$$v(a, y, z) - v(0, y, z) = \tfrac{1}{2} a$$

LIST OF REFERENCES

1. Cox, B.N. and Flanagan, G. "Handbook of Analytical Methods for Textile Composites," NASA CR-4750, Celveland, OH, 1997.

2. Tsai, S.W. and H.T. Hahn. *Introduction to Composite Materials,* Technomic Publishing Co, Lancaster, PA. 1980.

3. Dasgupta, A.S., S. Bhandarkar, M. Pecht, and D. Barkar. "Thermoelastic Properties of Woven-Fabric Composites using Homogenization Techniques," Proceedings of the American Society for Composites, Fifth Technical Conference, Lansing, MI, 1990. p1001-1010.

4. Foye, R.I. "Approximating the Stress Field within the Unit Cell of a Fabric Reinforced Composite Using Replacement Elements," NASA CR-191422, Cleveland, OH, 1993.

5. Naik, R.A. "Analysis of Woven and Braided Fabric Reinforced Composites," NASA CR-194930, Cleveland, OH, 1994.

6. Whitcomb, J.D. "Three-Dimensional Stress Analysis of Plain Weave Composites," Composite Materials Fatigue and Fracture (Third Volume), ASTM STP 1110, 1991. p417-438.

7. Ishikawa, T., and T.W. Chou, "One-dimensional Micromechanical Analysis of Woven Fabric Composites," *AIAA Journal*, Vol 21, 1983. p1714-1721.

8. Ma, C.L., J.M. Yang, and T.W. Chou, "Elastic Stiffness of Three-dimensional Braided Textile Structural Composites," Composite Materials: Testing and Design (7^{th} Conference), ASTM STP 893, 1986. p404-421.

9. Raju, I.S., R.L. Foye, and V.S. Avva, "A Review of Analytical Methods for Fabric and Textile Composites," Proceedings of the Indo-U.S. Workshop on Composite Materials for Aerospace Applications, Bangalore, India, Part I, 1990. p129-159.

10. Whitcomb, J.K. and K. Srirengan, "Effect of Various Approximations on Predicted Progressive Failure in Plain Weave Composites," *Composite Structures*, 34, 13-20, 1996.

11. Lomov, S.E. et al, "Textile Composites: Modelling Strategies," *Composites: Part A*, 32, 1379-1394, 2001.

12. Hochard, C., Aubourg, P.A., and Charles, J.P., "Modelling of the Mechanical Behavior of Woven-Fabric CFRP Laminates up to Failure," *Composites Science and Technology*, 61, 221-230, 2001.

13. Huang, Z.M. and Ramakrishna, S., "Modeling Inelastic and Strength Properties of Textile Laminates: A Unified Approach," *Composites Science and Technology*, 63, 445-466, 2002.

14. Bigaud, D. and Hamelin, P., "Stiffness and Failure Modelling of 2D and 3D Textile Reinforced Composites by Means of Imbricate Type Elements Approaches," *Computers and Structures*, 80, 2253-2264, 2002.

15. Woo, K. and Whitcomb, J.D., "A Post Processor Approach for Stress Analysis of Woven Textile Composites," *Composites Science and Technology*, 60, 693-704, 2000.

16. Tang, X. and Whitcomb, J.D., "General Techniques for Exploiting Periodicity and Symmetries in Micromechanics Analysis of Textile Composites," *Journal of Composite Materials*, vol 37, 13, 2003.

17. Cox, B.N., and M.S. Dadkhah, "A Binary Model of Textile Composites: I-Formulation," *Acta Metallurgica et Materiala*, 42, 10, 3463, 1994.

18. Yang, Q. and Cox, B.N., "Predicting Local Strains in Textile Composites Using the Binary Model Formulation," Proceedings of the ICCM 2003, San Diego, CA, July 2003.

19. Bogdanovich, A.E. and Pastore, C.M., "Material-Smart Analysis of Textile-Reinforced Structures," *Composites Science and Technology*, 56, 291-309, 1996.

20. Bogdanovich, A.E., "Multiscale Predictive Analysis of 3-D Woven Composites," SAMPE 35th International Technical Conference, Dayton, OH, September 2003.

21. Quek, S.C., Waas, A., et al. "Compressive Response and Failure of Braided Textile Composites: Part 2- Computations," *International Journal of Nonlinear Mechanics*, 39, 649-663, 2004.

22. Quek, S.C., Waas, A., et al. "Compressive Response and Failure of Braided Textile Composites: Part 1- Experiments," *International Journal of Nonlinear Mechanics*, 39, 635-648, 2004.

23. Cox, B.N., M.S. Dadkhah, and W.L. Morris, "Failure Mechanisms of 3D Woven Composites in Tension, Compression, and Bending," *Acta Metallurgica et Materiala*, 42, 12, 3967-84. 1994.

24. Pochiraju, K., T.W. Chou, and B.M. Shah, “Modeling Stiffness and Strength of 3D Textile Structural Composites,” Proceedings of the 37th Joint AIAA/ ASME/ ASCE/ AMS/ ASC Structures, Structural Dynamics, and Materials Conference, Salt Lake City, UT 1996.

25. Dadhkah, M.S., W.L. Morris, T. Kniveton, and B.N. Cox, “Simple Models for Triaxially Braided Composites,” *Composites*, 26, 1995. p91-102.

26. Fleck, N.A. and P.M. Jelf, “Deformation and Failure of a Carbon Fiber Composite under Combined Shear and Transverse Loading,” *Acta Metallurgica et Materiala,* 43, 8, 3001-7. 1995.

27. Swanson, S.R. and L.V. Smith, “Multiaxial Stiffness and Strength Characterization of 2D Braid Carbon/Epoxy Fiber Composites,” Mechanics of Textile Composites Conference, Hampton, VA, C.C. Poe, ed. NASA Conference Publication 3311. 1995.

28. Karkkainen, R.L. and B.V. Sankar, "A Direct Micromechanics Method for Failure Initiation of Plain Weave Textile Composites," *Composites Science and Technology*, 66, p137-150, 2006.

29. Zhu, H., B.V. Sankar, and R.V. Marrey, “Evaluation of Failure Criteria for Fiber Composites Using Finite Element Micromechanics,” *Journal of Composite Materials*, 32, 8, 1998. p766-782.

30. Marrey, R.V. and B.V. Sankar, “Micromechanical Models for Textile Structural Composites,” NASA CR-198229. Cleveland, OH, 1995.

31. Sankar, B.V. and R.V. Marrey, "Analytical Method for Micromechanics of Textile Composites," *Composites Science and Technology*, 57, 6, p703-713. 1997.

32. Marrey R.V. and B.V. Sankar, "A Micromechanical Model for Textile Composite Plates," *Journal of Composite Materials*, 31, 12, p1187-1213. 1997.

33. Carvelli V. and C. Poggi, “A Homogenization Procedure for the Numerical Analysis of Woven Fabric Composites,” *Composites Part A: Applied Science and Manufacturing*, 32, 1425-1432, 2001.

34. Gibson, R.F. *Principles of Composite Material Mechanics*, McGraw-Hill, Inc, New York, 1994.

35. Whitcomb, J.D., C.D. Chapman, and K. Srirengan, “Analysis of Plain-Weave Composites Subjected to Flexure,” *Mechanics of Composite Materials and Structures*, 5:41-53, 1998.

36. Whitney, J.M. *Structural Analysis of Laminated Anisotropic Plates*, Technomic Publishing Co, Lancaster, PA, 1987.

37. Norton, R.L. *Machine Design: An Integrated Approach*, Prentice-Hall Inc, Upper Saddle River, NJ, 1996.